Bulletin of Engineering Geology and the Environment (2019) 78:4397–4419
https://doi.org/10.1007/s10064-018-1401-8

ORIGINAL PAPER

Novel hybrid artificial intelligence approach of bivariate statistical-methods-based kernel logistic regression classifier for landslide susceptibility modeling

Wei Chen[1,2] · Himan Shahabi[3] · Ataollah Shirzadi[4] · Haoyuan Hong[5,6,7] · Aykut Akgun[8] · Yingying Tian[9] · Junzhi Liu[5,6,7] · A-Xing Zhu[5,6,7] · Shaojun Li[10]

Received: 25 March 2018 / Accepted: 4 October 2018 / Published online: 9 November 2018

Abstract
Globally, and in China, landslides constitute one of the most important and frequently encountered natural hazard events. In the present study, landslide susceptibility evaluation was undertaken using novel ensembles of bivariate statistical-methods-based (evidential belief function (EBF), statistical index (SI), and weights of evidence (WoE)) kernel logistic regression machine learning classifiers. A landslide inventory comprising 222 landslides and 15 conditioning factors (slope angle, slope aspect, altitude, plan curvature, profile curvature, stream power index, sediment transport index, topographic wetness index, distance to rivers, distance to roads, distance to faults, NDVI, land use, lithology, and rainfall) was prepared as the spatial database. Correlation analysis and selection of conditioning factors were conducted using multicollinearity analysis and classifier attribute evaluation methods, respectively. The receiver operating characteristic curve method was used to validate the models. The areas under the success rate (AUC_T) and prediction rate (AUC_P) curves and landslide density analysis were also used to assess the prediction capability of the landslide susceptibility maps. Results showed that the EBF-KLR hybrid model had the highest predictive capability in landslide susceptibility assessment (AUC values of 0.814 and 0.753 for the training and validation datasets, respectively; AUC_T value of 0.8511 and AUC_P value of 0.7615), followed in descending order by the SI-KLR and WoE-KLR hybrid models. These findings indicate that hybrid models could improve the predictive capability of bivariate models, and that the EBF-KLR is a promising hybrid model for the spatial prediction of landslides in susceptible areas.

Keywords Landslides · Bivariate models · Kernel logistic regression · GIS · China

✉ Wei Chen
chenwei.0930@163.com; chenwei0930@xust.edu.cn

✉ Haoyuan Hong
honghaoyuan333@gmail.com; hong_haoyuan@outlook.com

1 College of Geology & Environment, Xi'an University of Science and Technology, Xi'an 710054, Shaanxi, China

2 Shandong Provincial Key Laboratory of Depositional Mineralization & Sedimentary Minerals, Shandong University of Science and Technology, Qingdao 266590, China

3 Department of Geomorphology, Faculty of Natural Resources, University of Kurdistan, Sanandaj, Iran

4 Department of Rangeland and Watershed Management, Faculty of Natural Resources, University of Kurdistan, Sanandaj, Iran

5 Key Laboratory of Virtual Geographic Environment (Nanjing Normal University), Ministry of Education, Nanjing 210023, China

6 State Key Laboratory Cultivation Base of Geographical Environment Evolution (Jiangsu Province), Nanjing 210023, China

7 Jiangsu Center for Collaborative Innovation in Geographic Information Resource Development and Application, Nanjing 210023, Jiangsu, China

8 Geological Engineering Department, Karadeniz Technical University, Trabzon, Turkey

9 Key Laboratory of Active Tectonics and Volcano, Institute of Geology, China Earthquake Administration, #1 Huayanli, Chaoyang District, PO Box 9803, Beijing 100029, People's Republic of China

10 State Key Laboratory of Geomechanics and Geotechnical Engineering, Institute of Rock and Soil Mechanics, Chinese Academy of Sciences, Wuhan 430071, Hubei, China

Introduction

Landslides are important natural hazard events that occur frequently in China and around the world. Steep topography, heavy precipitation, weak lithological units, adverse anthropologic treatments to land, and earthquakes are among the factors primarily responsible for landslide occurrence (Althuwaynee et al. 2015; Hong et al. 2017; Ma et al. 2015; Yuan et al. 2013, 2015, 2016). Because the occurrence location, size, and volume of landslides are reasonably predictable parameters, the potential for mitigation of their adverse effects is much greater compared with earthquakes. Specifically, landslide susceptibility maps that show the spatial occurrence probability of such events have been used for regional land use management by decision makers because of their effectiveness and ease of production. In this context, many studies conducted in the last two decades have focused on landslide susceptibility mapping.

Close inspection of published reports of landslide susceptibility studies reveals that several datasets and assessment methodologies have been developed and discussed (Broeckx et al. 2018; Hong et al. 2018; Pham et al. 2018; Pourghasemi and Rahmati 2018; Reichenbach et al. 2018; Shirzadi et al. 2017). Although there is no consensus regarding the optimal dataset and assessment methodology, some datasets (e.g., slope angle, lithology, and land use/cover) have been accepted widely as fundamental in landslide susceptibility mapping (Youssef et al. 2015). Certain assessment methodologies have also been adopted in many landslide susceptibility studies, e.g., the analytical hierarchy process (Kumar and Anbalagan 2016; Pourghasemi and Rossi 2016), frequency ratio (Regmi et al. 2014; Wang et al. 2016), statistical index (SI) (Nasiri Aghdam et al. 2016; Zhang et al. 2016a), evidential belief function (EBF) (Ding et al. 2017; Pourghasemi and Kerle 2016; Zhang et al. 2016b), logistic regression (LR) (Raja et al. 2017; Tsangaratos et al. 2017), and weights of evidence (WoE) (Ding et al. 2017; Wang et al. 2016). Given this variety in datasets and methodologies, it is important to compare the results obtained by different methods and datasets to determine the optimal combination.

In addition to the above statistical methods, more sophisticated machine learning methods, such as artificial neural networks (Chen et al. 2017b; Tien Bui et al. 2016; Yilmaz 2010), kernel logistic regression (KLR) (Tien Bui et al. 2016), support vector machine (Chen et al. 2017c; Pham et al. 2015; Pradhan 2013; Tien Bui et al. 2016), random forests (Chen et al. 2017g; Hong et al. 2016; Pourghasemi and Kerle 2016), decision trees (Althuwaynee et al. 2014; Hong et al. 2015; Pradhan 2013), multivariate adaptive regression splines (Chen et al. 2017d; Pourghasemi and Rossi 2016), and derivative approaches of artificial neural networks (Chen et al. 2017a; Nasiri Aghdam et al. 2016; Pradhan 2013; Tien Bui et al. 2012) have also become popular assessment methodologies through integration with developing GIS technologies.

Two of the major drawbacks of bivariate statistical approaches, such as EBF, SI, and WOE, are that strict assumptions must be defined prior to conducting any study (Benediktsson et al. 1989) and that the relationships between conditioning factors are largely neglected. Conversely, machine learning methods do not require any statistical assumptions and they are capable of handling data with various measurement scales; however, they cannot be used to evaluate the relationships between individual factor classes and landslides.

Given the above, it may be concluded that complex and nonlinear problems could be handled using ensemble methods (Tehrany et al. 2014). In this context, the main aim of this study was to investigate the effectiveness of the ensemble methodologies of KLR with bivariate EBF, SI, and WoE models based on comparison of the results obtained. The second purpose, of course, was to build a landslide susceptibility map for the study area that could be used by local decision makers for effective land use planning purposes. The investigation of the use of the EBF, SI, WoE, and KLR ensembles constitutes the novelty of this study.

Materials and methods

The methodology design comprised five steps: (1) spatial data preparation including landslide inventory and conditioning factors; (2) estimation of the EBF, SI, and WOE methods; (3) selection of conditioning factors; (4) construction of landslide susceptibility maps using three bivariate models and three ensemble models; and (5) assessment and validation of model performance (Fig. 1).

Study area

The study area (Chongren County), which is located in the region 27°25′N–27°56′N, 115°49′E–116°17′E, covers an area of about 1520 km^2 in Jiangxi Province (China) (Fig. 2). Chongren County has a subtropical monsoon climate. The average annual temperature is 17.7 °C (Hong et al. 2017). The high frequency of intense rainfall during April–August accounts for 79.5% of the annual total. The average rainfall in May and June is 265 and 305 mm, respectively.

The rivers in Chongren County belong to the Fu River system. The total flow path is up to 910 km, and the drainage density is 0.6 km^{-2}. The main rivers within the study area are the Chongren and Yihuang rivers. Geologically, the Chongren area is located within the depression belt uplift in central–

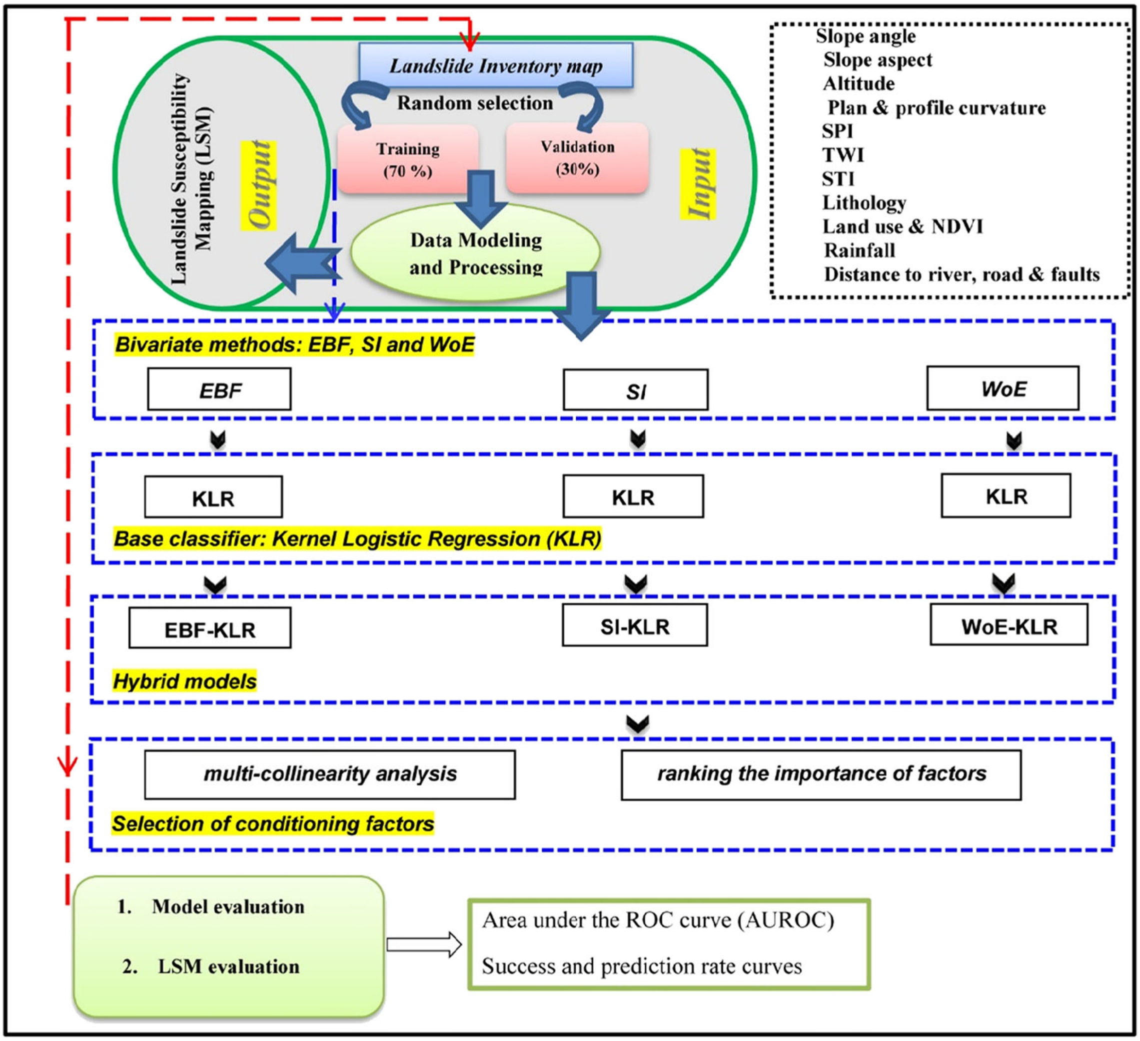

Fig. 1 Flowchart of the used methodology

southern Jiangxi Province, and it is a transition zone between the Yu Mountains and the Gan-Fu Plain. The strata outcropped in the study area are mainly pre-Sinian, Sinian, Cambrian, Carboniferous, Triassic, Jurassic, Cretaceous, and Quaternary. The main lithologies are limestone, shale, sandstone, slate, and igneous rocks (Fig. 3).

Database

Landslide inventory

The compilation of a landslide inventory is the first step in landslide susceptibility modeling, and various methods for this process have been applied in different studies (Harp et al. 2011; Moosavi et al. 2014). Landslide inventory maps are effective and easily comprehensible products for geomorphologists, decision makers, planners, and civil defense managers (Galli et al. 2008). However, the advantages and limitations of applying new remote sensing data and technologies in the production of landslide inventory maps have been discussed in previous work (Guzzetti et al. 2012). Thus, in light of the above analysis, this study adopted field surveys, historical records, and high-resolution satellite images coupled with Google Earth™ technology to produce the landslide inventory map.

In the current study, 222 landslide events were identified and mapped with projected area in the Chongren area. Through investigation of the landslide inventory map, the largest landslide was found to be 15,000 m^2, the smallest landslide was 2.5 m^2, and the average was 841.3 m^2 (Hong et al. 2017). In the Chongren area, local government reports show only 19.1% of the total number of landslides are large-sized landslides (>800 m^2) that affect 1365 people (http://www.jxcr.gov.cn/). Medium-sized (200–800 m^2) landslides account for 25.4% of the total, and they affect 1019 people. Small-sized landslides (<200 m^2) account for 55.5% of the total, and they affect 875 people.

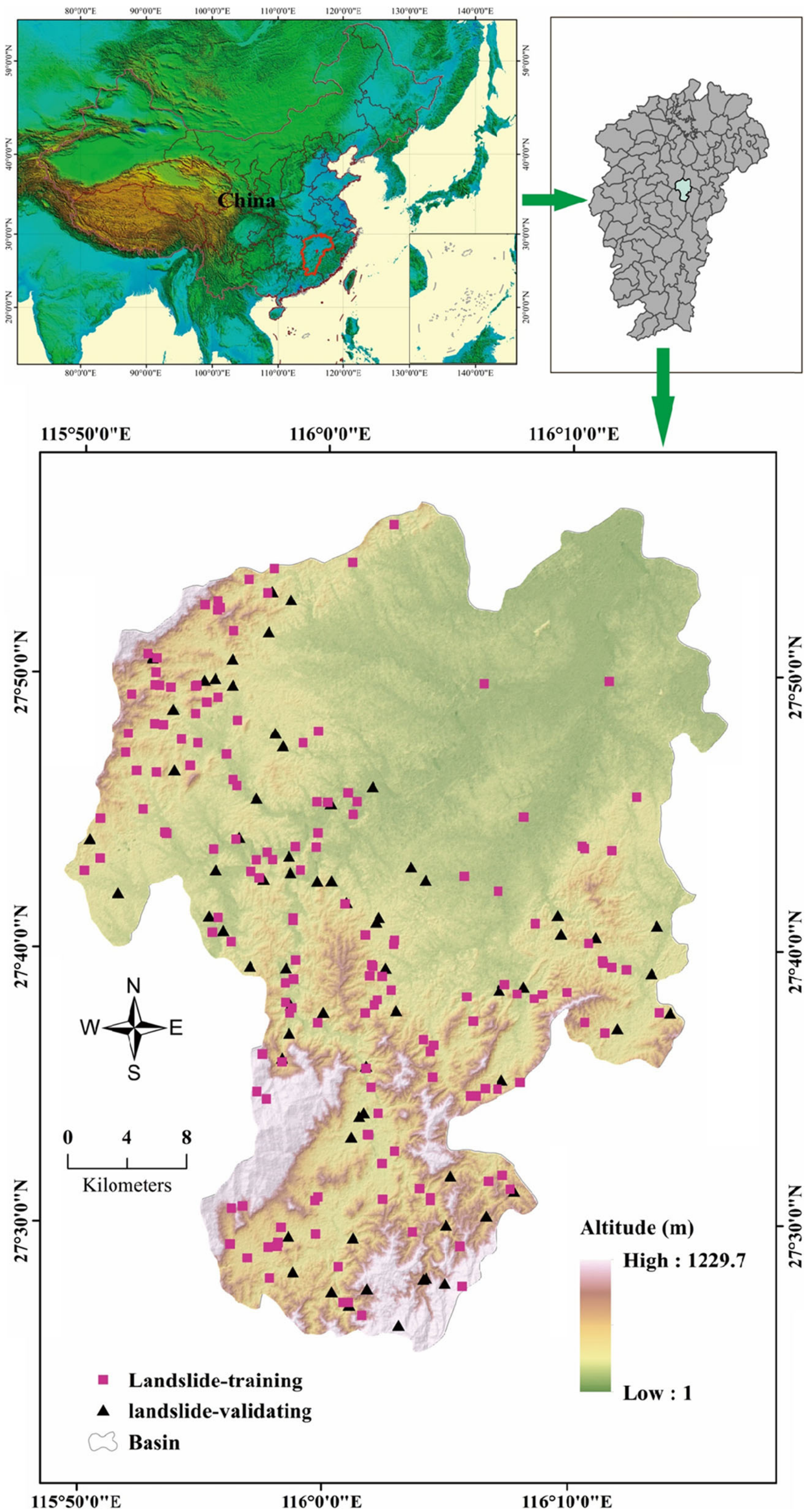

Fig. 2 Location map of the study area

Conditioning factors

The causes of landslide development and occurrence are complex and diverse, and there is no clear agreement with respect to the precise reasons for their manifestation (Domínguez-Cuesta et al. 2007). The complex nature of the development of landslides (Jiménez Sánchez et al. 1999) has caused many researchers to investigate how landslide occurrence might be

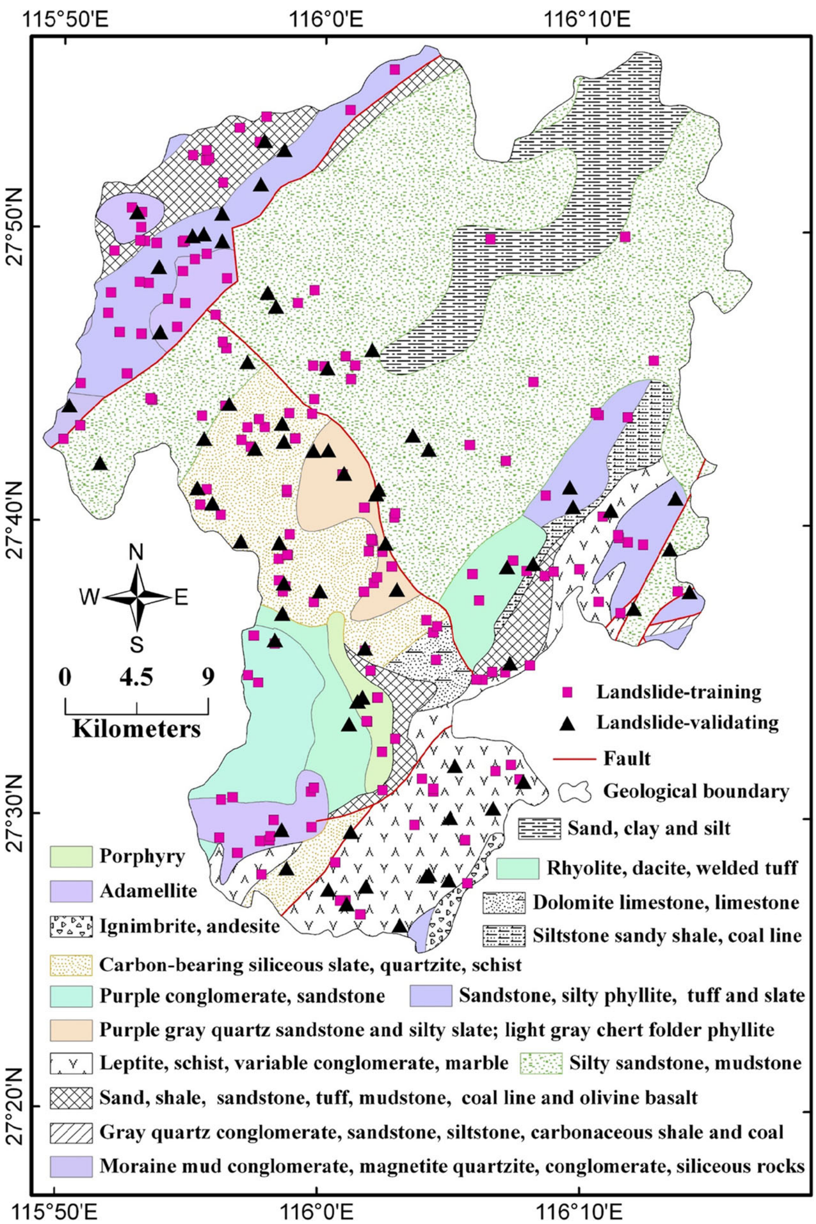

Fig. 3 Geological map of the study area

affected by various conditioning factors, e.g., the topographical, geological, and environmental conditions (Zêzere et al. 1999). Therefore, the selection of appropriate conditioning factors is a challenging task. Some previous studies have assumed that the use of increased numbers of conditioning factors would enhance the precision of a landslide susceptibility map (van Westen et al. 2003). However, other research has indicated that conditioning factors with reasonable quality are necessary for producing accurate landslide susceptibility maps (Jebur et al. 2014). Thus, according to a literature review (Broeckx et al. 2018; Pourghasemi 2014; Reichenbach et al. 2018) and our actual analysis of the geo-environmental characteristics of the study area and data availability, this study considered 15 landslide conditioning factors that were grouped into three categories: topographical, geological, and environmental.

Topographical factors Topographical factors, such as slope angle, slope aspect, altitude, plan curvature, profile curvature, stream power index (SPI), sediment transport index (STI), and topographic wetness index (TWI), were derived based on 1:50,000 topographic maps (http://www.jxgtt.gov.cn/). Among them, slope angle was used to classify the degree of steepness of hills and mountains (Iwahashi et al. 2003). The initial slope angle is an important factor that affects the peak strength of the slope material, and it controls the source of material available for landslides (Chen et al. 2016). Therefore, in this study, slope was selected as a conditioning factor.

Slope aspect is defined as the direction in which a slope faces and it relates to the degree of solar exposure. Aspect also influences both the vegetation coverage and the daily ranges of temperature and relative humidity of a slope (Jonathan et al. 2006). Many articles have discussed the relationship between slope aspect and landslides; however, there is a lack of consensus regarding its adoption as a conditioning factor. Because slope aspect has been shown to influence landslides triggered by rainfall (Beullens et al. 2014), slope aspect was selected as a conditioning factor in this study.

Altitude is defined as the elevation above a ground reference point, which is commonly the terrain elevation. Altitude is considered an important landslide conditioning factor because of its gravitational potential energy.

Plan curvature influences the convergence and divergence of flow across a surface. Profile curvature affects the acceleration and deceleration of downslope flows, and it influences the processes of erosion and deposition (Kritikos and Davies 2015). These two factors were also accepted as conditioning factors in this study.

SPI is a term that describes the potential flow erosion of the topographic surface at a given point. STI also characterizes the processes of erosion and deposition. TWI can be used to quantify the effects of hydrological processes in relation to topography. Therefore, these three factors were also accepted as conditioning factors.

Geological factors The lithological data were collected from the China Geology Survey (http://www.cgs.gov.cn/) (1: 200,000 scale). The lithology map was reclassified into ten groups according to their geological ages and lithofacies (Hong et al. 2017). The distance to fault map was constructed by generating buffers along the fault lines using ArcGIS software (ESRI 2014).

Environmental factors The NDVI was derived from Landsat-8 Operational Land Imagery (Path/Row: 121/41; date: November 01, 2017; Product ID: LC81210412017305LGN00; available at http://www.gscloud.cn). The value of the NDVI was estimated using the formula: NDVI = $(NIR - R)/(NIR + R)$, where NIR and R are the near-infrared band and red band, respectively. The land use map was also obtained from the same Landsat 7/ETM+ satellite images. Land use was classified into six categories: residential, bare, water, forest, farmland, and grass. The distance to rivers and the distance to roads maps were also constructed by buffering 1:50,000-scale topographic maps.

The rainfall data were provided by the Jiangxi Province Meteorological Bureau (http://www.weather.org.cn). The mean annual precipitation data for the period of 1960–2012 at 18 rainfall stations were used to construct the rainfall map by application of the inverse distance weighted method (Hong et al. 2017).

Finally, all landslide conditioning factors were converted into raster format with 25-m spatial resolution for application with the models (Fig. 4a–o). The detailed classification of the landslide conditioning factors is shown in Table 1. The area grid comprised 2286 rows by 1782 columns, which corresponded to 2,427,151 cells, 222 of which included landslide occurrences.

Methods

Evidential belief function (EBF)

In 1967, Dempster first proposed the basis of the Dempster–Shafer theory of evidence (Dempster 1967), which was developed further by Shafer in 1976 (Shafer 1976). This method incorporates four basic EBFs: degrees of belief (Bel), disbelief (Dis), uncertainty (Unc), and plausibility (Pls), of which Bel = low probability and Pls = upper probability constitute the main elements of the theory (Dempster 1967). Unc represents the ignorance of one's belief in a proposition based on given evidence and its value is $Pls - Bel$. Dis is the belief that a proposition is not true based on given evidence, the value of which is equal to $1 - Pls$ or $1 - Bel - Unc$. The EBF method is popular in many fields of study, such as forest fire susceptibility mapping (Pourghasemi 2016), landslide susceptibility mapping (Ding et al. 2017; Pourghasemi and Kerle 2016; Pradhan et al. 2014; Tien Bui et al. 2015), and groundwater potential mapping (Mogaji et al. 2016; Tahmassebipoor et al. 2016). The estimation of EBFs can be calculated as follows:

$$Bel(Cij) = \frac{W_{C_{ij(landslide)}}}{\sum_{j=1}^{n} W_{C_{ij(landslide)}}}, \tag{1}$$

$$W_{C_{ij}(landslide)} = \frac{N\left(T \cap C_{ij}\right)/N(T)}{\left[N\left(C_{ij}\right) - N\left(T \cap C_{ij}\right)\right]/[N(C) - N(T)]}. \tag{2}$$

The numerator in Eq. (2) is the proportion of landslide pixels that occur in factor class C_{ij}, and the denominator is the proportion of non-landslide pixels that occur in factor class C_{ij}. $W_{C_{ij(landslide)}}$ is the weight of C_{ij} that supports the belief that landslides are present more than absent.

$$W_{C_{ij}(non-landslide)} = \frac{\left[N\left(C_{ij}\right) - N\left(T \cap C_{ij}\right)\right]/N(T)}{\left[N(C) - N(T) - N\left(C_{ij}\right) + N\left(T \cap C_{ij}\right)\right]/[N(C) - N(T)]}. \tag{3}$$

The numerator in Eq. (3) is the proportion of landslide pixels that do not occur in factor class C_{ij}, and the denominator is the proportion of non-landslide pixels in other attributes outside factor class C_{ij}. $W_{C_{ij}(non-landslide)}$ is the weight of C_{ij} that supports the belief that landslides are absent more than present. Therefore, we have the following equations:

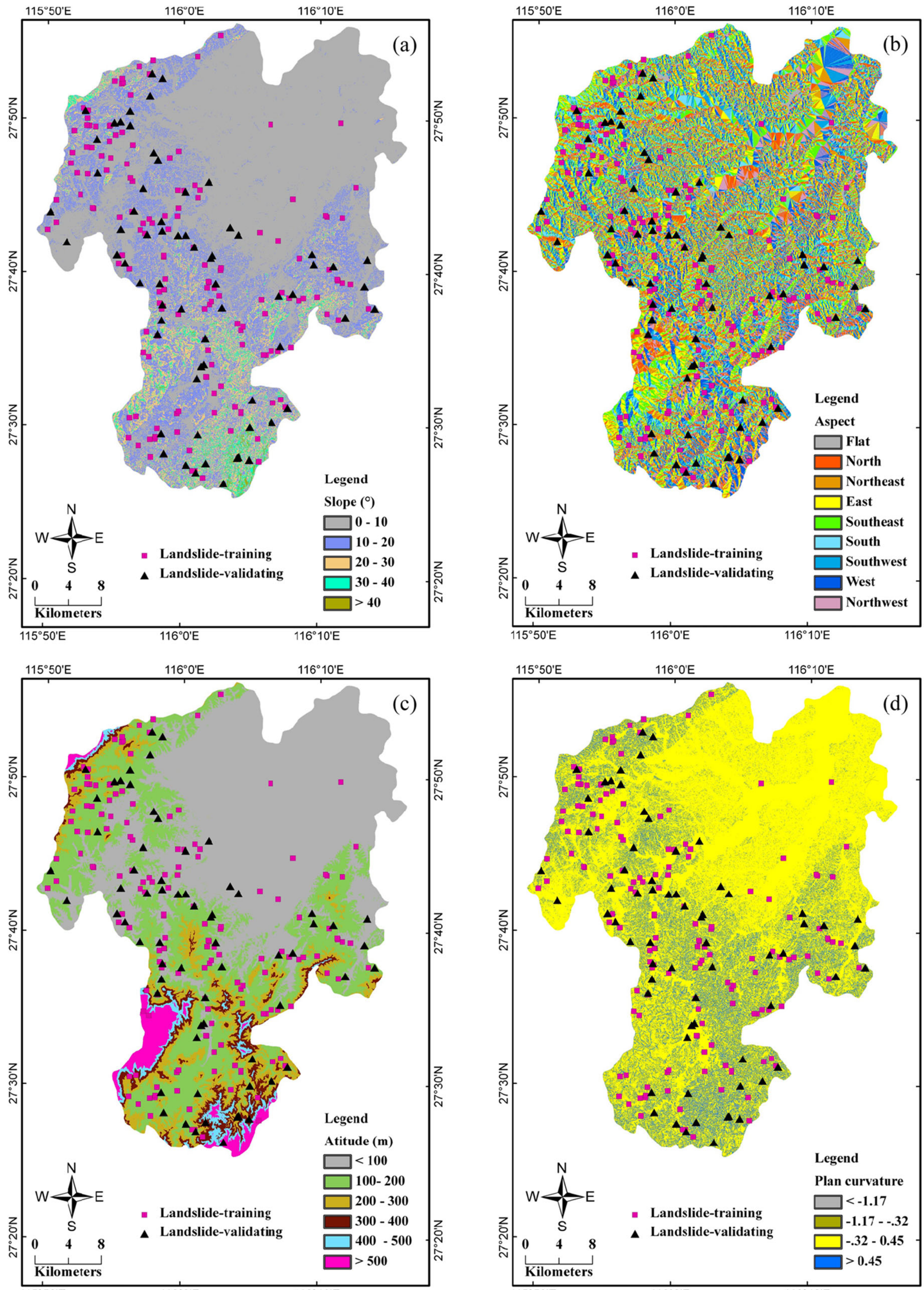

Fig. 4 Thematic maps of the study area: (**a**) Slope angle; (**b**) Slope aspect; (**c**) Altitude; (**d**) Plan curvature; (**e**) Profile curvature; (f) SPI; (**g**) STI; (h) TWI; (**i**) Distance to rivers; (**j**) Distance to roads; (**k**) Distance to faults; (**l**) NDVI; (m) Landuse; (**n**) Lithology; (**o**) Rainfall

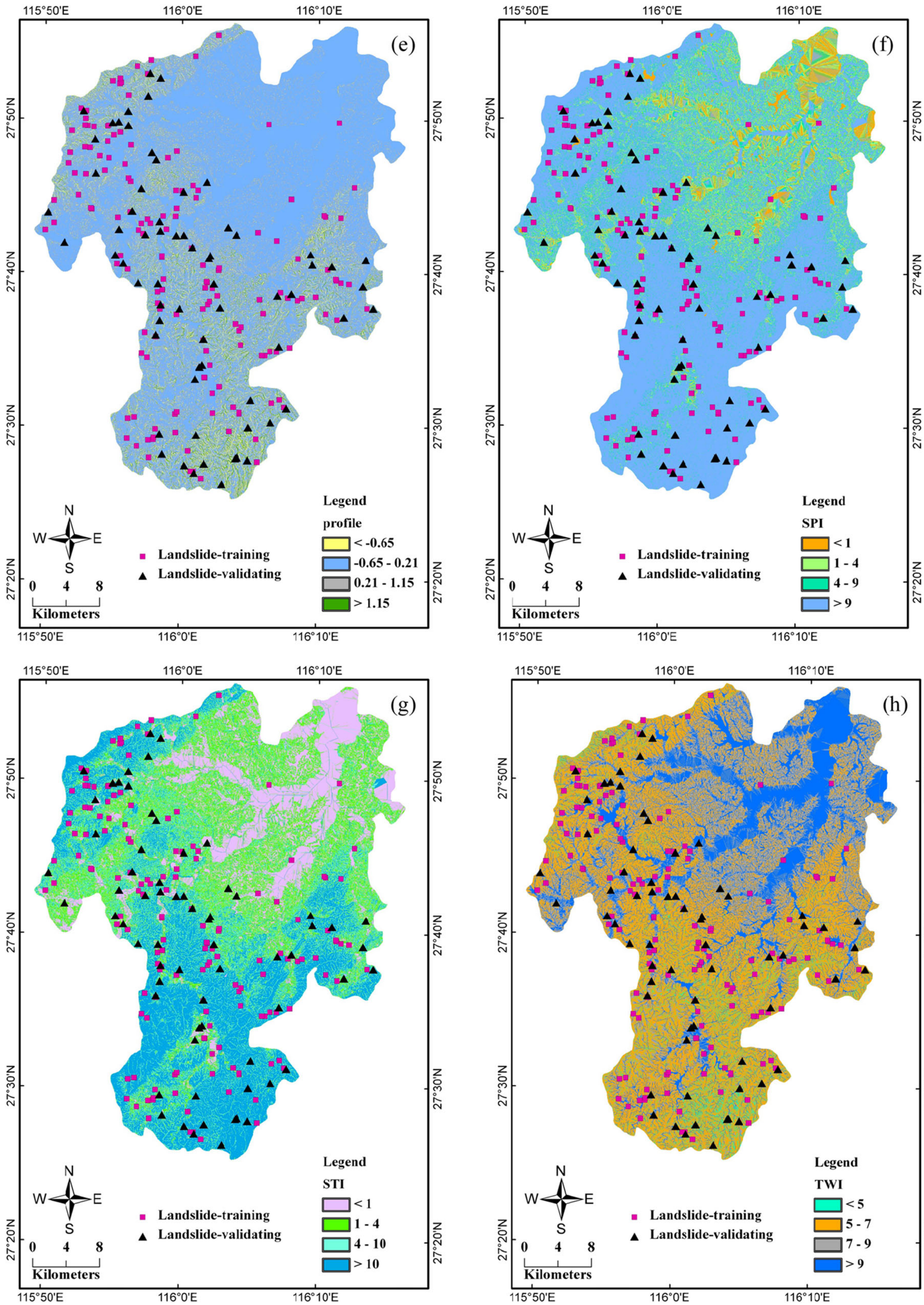

Fig. 4 (continued)

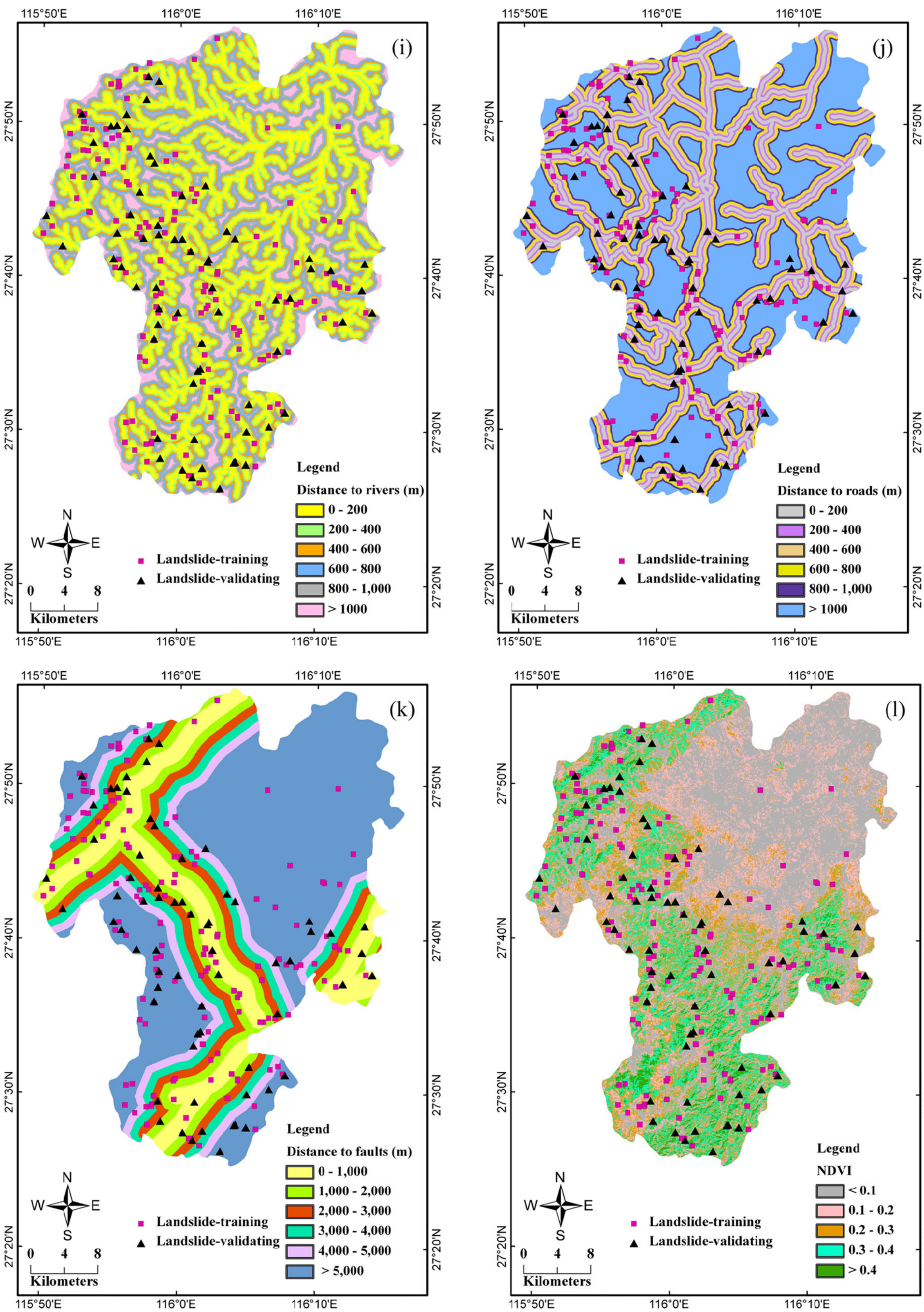

Fig. 4 (continued)

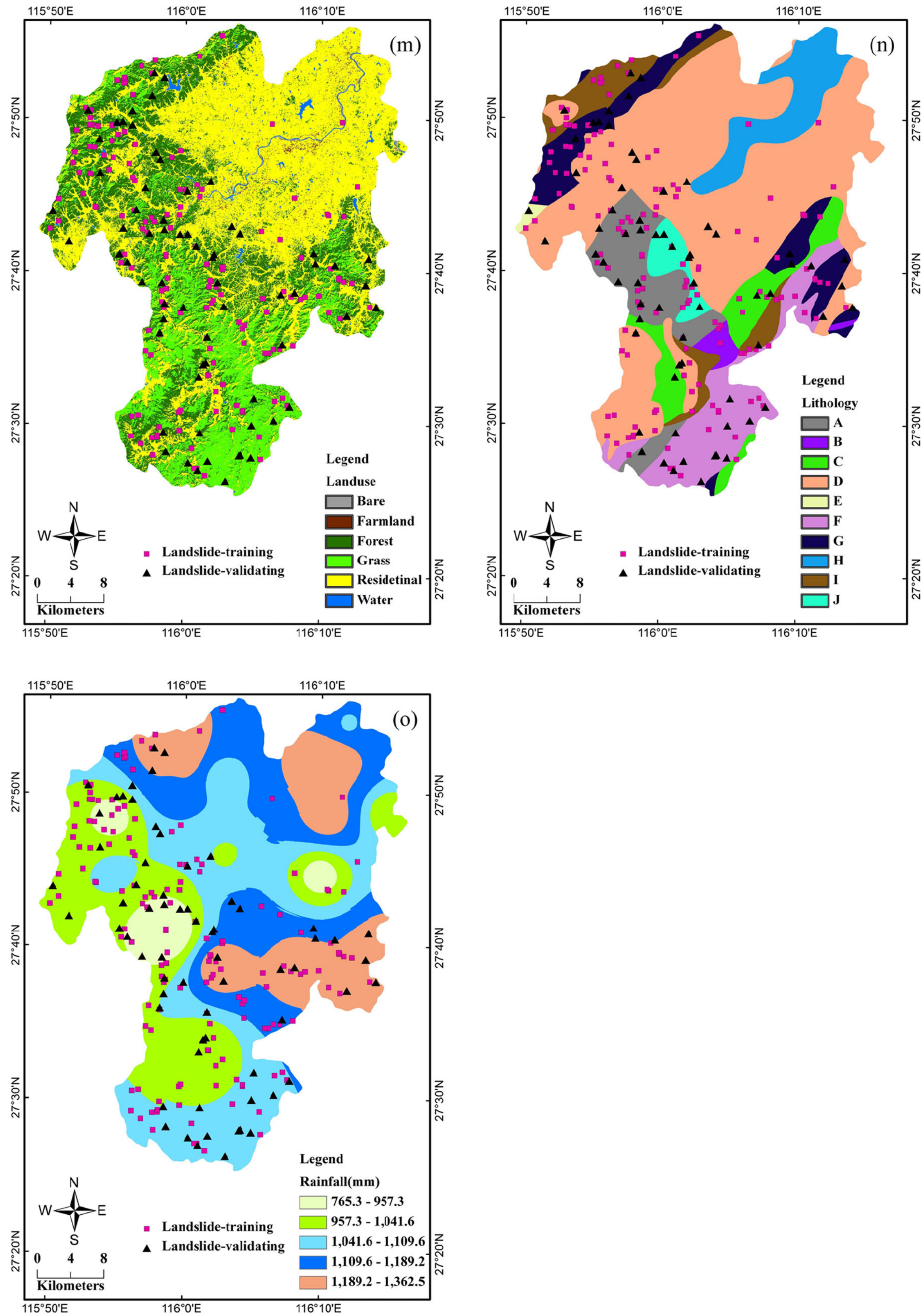

Fig. 4 (continued)

Table 1 Classes of landslide conditioning factors

Conditioning factors	Classes
Slope angle (°)	(1) 0–10; (2) 10–20; (3) 20–30; (4) 30–40; (5) > 40
Slope aspect	(1) Flat; (2) North; (3) Northeast; (4) East; (5) Southeast; (6) South; (7) Southwest; (8) West; (9) Northwest
Altitude (m)	(1) < 1,00; (2) 1,00–200; (3) 200–300; (4) 300–400; (5) 400–500; (6) > 500
Plan curvature	(1) < −1.17; (2) −1.17–−0.32; (3) −0.32–0.45; (4) > 0.45
Profile curvature	(1) < −0.65; (2) −0.65–0.21; (3) 0.21–1.15; (4) > 1.35
SPI	(1) < 1; (2) 1–4; (3) 4–9; (4) > 9
STI	(1) < 1; (2) 1–4; (3) 4–10; (4) > 10
TWI	(1) < 5; (2) 5–7; (3) 7–9; (4) > 9
Distance to rivers (m)	(1) 0–200; (2) 200–400; (3) 400–600; (4) 600–800; (4) 800–1000; (6) > 1000
Distance to roads (m)	(1) 0–200; (2) 200–400; (3) 400–600; (4) 600–800; (4) 800–1000; (6) > 1000
Distance to faults (m)	(1) 0–1000; (2) 1000–2000; (3) 2000–3000; (4) 3000–4000; (5) > 4000
NDVI	(1) < 0.1; (2) 0.1–0.2; (3) 0.2–0.3; (4) 0.3–0.4; (5) > 0.4
Land use	(1) Bare; (2) Farmland; (3) Forest; (4) Grass; (5) Residential; (6) Water
Lithology	(1) A; (2) B; (3) C; (4) D; (5) E; (6) F; (7) G; (8) H; (9) I; (10) J
Rainfall (mm/yr)	(1) 765.3–957.3; (2) 957.3–1041.6; (3) 1041.6–1109.6; (4) 1109.6–1189.2; (5) 1189.2–1362.5

$$Dis\left(C_{ij}\right) = \frac{W_{C_{ij}(non-landslide)}}{\sum_{j=1}^{n} W_{C_{ij(non-landslide)}}}, \tag{4}$$

$$Unc_{Cij} = 1 - Bel_{Cij} - Dis_{Cij}, \tag{5}$$

$$Pls_{Cij} = Bel_{Cij} + Unc_{Cij}. \tag{6}$$

Statistical index (SI)

The SI was proposed by van Westen (1997). In the SI method, a weight value of a parameter class is characterized by the natural logarithm of the landslide density in the class divided by the landslide density in the entire map. The equation to calculate the weights is as follows (van Westen 1997):

$$W_{SI} = \ln\left(\frac{Densclass}{Densmap}\right) = \ln\left[\frac{N(Si)}{N(Ni)} \Big/ \frac{\sum N(Si)}{\sum N(Ni)}\right], \tag{7}$$

where W_{SI} is the weight for the given parameter class, *Densclass* is the landslide density within the parameter class, and *Densmap* is the landslide density within the entire map. $N(Si)$ is the number of landslide pixels in parameter class i, and $N(Ni)$ is the number of pixels in the same parameter class.

Weights of evidence (WoE)

As one of the most popular models, the WOE method adopts the Bayesian theory of conditional probability to quantify spatial associations between evidence layers and known mineral occurrences (Agterberg 1989; Bonham-Carter 1994). In this study, we use the WOE for modeling large-scale landslide susceptibility spatial prediction. Recently, many researchers have applied WoE in various ways, such as mineral prospective mapping (Zeghouane et al. 2016), flood susceptibility (Rahmati et al. 2016), landslide susceptibility mapping (Ding et al. 2017), and groundwater potential (Mogaji et al. 2016; Tahmassebipoor et al. 2016). It is worth noting that conditional independence is the most important issue to be considered in the WOE method (Zhang et al. 2014). Hence, the WOE is determined by the calculation of positive and negative weights W^+ and W^-, which can be expressed as follows:

$$W^+ = \ln\frac{p\{B|A\}}{p\left\{B|\overline{A}\right\}}, \tag{8}$$

$$W^- = \ln\frac{p\left\{\overline{B}|A\right\}}{p\left\{\overline{B}|\overline{A}\right\}}. \tag{9}$$

In the above two equations, p represents the probability, ln is the natural log, B is the presence of a potential landslide predictive factor, $\overline{B}$ is the absence of a potential landslide predictive factor, A is the presence of a landslide, and $\overline{A}$ is the absence of a landslide. Thus, W^+ indicates that the predictable variable is present at the landslide locations and W^- indicates the absence of the predictable variable. In landslide susceptibility prediction, we use the studentized contrast $C/S(C)$ to measure and reflect the spatial association between the landslide conditioning factors and landslide occurrence, where C is the weight contrast and $S(C)$ is the standard deviation of C. These can be expressed as follows:

$$C = W^{+} - W^{-}, \tag{10}$$

$$S(C) = \sqrt{S^2W^{+} + S^2W^{-}}, \tag{11}$$

where S^2W^+ is the variance of the positive weights and S^2W^- is the variance of the negative weights.

Kernel logistic regression (KLR)

KLR is one type of logistic regression that applies kernel theory. The main aim of this approach is to classify a large quantity of data in a high-dimensional space because it might be difficult to distinguish in the current dimensional space using a linear logistic regression model (Cawley and Talbot 2005; Tien Bui et al. 2016). We can express the KLR as follows:

$$\mathrm{log}it\{p\} = w \cdot \varphi(u) + c, \tag{12}$$

where w is the vector of the landslide conditioning factors, $\varphi(u)$ is a nonlinear transformation to each input variable, and c is a bias term. For convenience, $\varphi(u)$ can be simply calculated, i.e., the cause $\varphi(u)\varphi^{'}(u)$ is a certain outcome during the calculation procedure, which evaluates the inner product between the image of input vectors in the feature space:

$$K\left(u, u^{'}\right) = \varphi(u) \cdot \varphi^{'}(u). \tag{13}$$

For a kernel to support the interpretation as an inner product in a fixed feature space, the kernel must obey Mercers' condition (Mercer 1909). Many kernel functions have been suggested, such as the radial basis function (RBF) and the linear kernel (Lin and Lin 2003). In this study, KLR was used to describe the problem:

$$K\left(u, u^{'}\right) = e^{\left[\frac{-\|u-u'\|^2}{2\delta^2}\right]}, \tag{14}$$

where δ is a turning parameter that controls the sensitivity of the kernel. According to the represented theorem (Kimeldorf and Wahba 1971; Schölkopf et al. 2001), vector w can be determined by minimizing a cost function, which can be expressed as follows:

$$w = \sum_{i-1}^{n} \alpha_i \varphi(u) \tag{15}$$

where $\alpha_{i,i}$=(1,2,…,n) is the vector of the landslide conditioning factors. Thus, we obtain the following formula:

$$\mathrm{log}it\{p\} = \sum_{i-1}^{n} \alpha_i K\left(u, u^{'}\right) + c. \tag{16}$$

Construction of training and validation datasets

The values of 15 conditioning factors for the three bivariate models were extracted to the landslide inventory in this study. Landslide locations (grid pixels) were assigned to 1, whereas the same number of non-landslide locations (grid pixels) outside the landslides were assigned to 0. To evaluate the prediction capability of landslide susceptibility models, the landslide inventory and non-landslide dataset should be divided into two subsets, i.e., the training and validation sets (Chung and Fabbri 2003). Therefore, the landslide inventory and non-landslide dataset were split randomly into two parts with a ratio of 70:30 to construct and validate the models, respectively. There were 155 landslide locations and 155 non-landslide locations in the training dataset, while the validation dataset had 67 landslide locations and 67 non-landslide locations.

Correlation analysis of conditioning factors

As the ensemble models are a combination of KLR developed from logistic regression, the assessment of correlation among the landslide conditioning factors is an important issue. There are two parameters for assessing the multicollinearity analysis: tolerance (TOL) and the variance inflation factor (VIF) (Chen et al. 2017f).

$$TOL = 1 - R^2, \tag{17}$$

$$VIF = 1/TOL. \tag{18}$$

According to the literature, a TOL of less than 0.20 or 0.10 and/or a VIF of more than 5 or 10 implies a multicollinearity problem (O'Brien 2007).

Model performance and validation of landslide susceptibility maps

The performances of three landslide ensemble models were evaluated using the receiver operating characteristic (ROC) curve. The area under the ROC curve (AUC) is a significant measurement for the assessment of the prediction capability of models in landslide modeling (Tien Bui et al. 2016). When the AUC is equal to 1, an ideal model is acquired (Chen et al. 2017e). The AUC can be computed using the following equation:

Table 2 Spatial relationship between each landslide conditioning factor and landslide by EBF, SI, and WoE models

Factors	Classes	Percentage of domain (%)	Percentage of landslide (%)	FR	Bel	Dis	Unc	Pls	SI	C	*S(C)*	*C/S(C)*
Slope angle (°)	<10	60.933	41.935	0.688	0.117	0.284	0.599	0.716	−0.374	−0.770	0.163	−4.730
	10–20	22.894	42.581	1.860	0.316	0.142	0.542	0.858	0.621	0.915	0.162	5.635
	20–30	12.603	12.258	0.973	0.165	0.192	0.643	0.808	−0.028	−0.032	0.245	−0.129
	30–40	3.154	2.581	0.818	0.139	0.192	0.669	0.808	−0.201	−0.207	0.507	−0.408
	>40	0.416	0.645	1.550	0.263	0.190	0.546	0.810	0.439	0.442	1.003	0.440
Slope aspect	Flat	0.700	0.000	0.000	0.000	0.000	1.000	1.000	0.000	0.000	0.000	0.000
	North	11.344	6.452	0.569	0.070	0.117	0.812	0.883	−0.564	−0.618	0.327	−1.891
	Northeast	13.044	14.839	1.138	0.141	0.109	0.750	0.891	0.129	0.150	0.226	0.663
	East	14.587	12.258	0.840	0.104	0.114	0.782	0.886	−0.174	−0.201	0.245	−0.820
	Southeast	12.836	16.774	1.307	0.162	0.106	0.732	0.894	0.268	0.314	0.215	1.460
	South	11.021	14.839	1.346	0.167	0.106	0.727	0.894	0.297	0.341	0.226	1.511
	Southwest	11.756	8.387	0.713	0.088	0.115	0.796	0.885	−0.338	−0.375	0.290	−1.295
	West	12.824	11.613	0.906	0.112	0.113	0.775	0.887	−0.099	−0.113	0.251	−0.451
	Northwest	11.887	14.839	1.248	0.155	0.107	0.738	0.893	0.222	0.256	0.226	1.132
Altitude	< 100	52.093	34.194	0.656	0.150	0.226	0.625	0.774	−0.421	−0.739	0.169	−4.361
	100–200	29.564	55.484	1.877	0.428	0.104	0.469	0.896	0.630	1.088	0.162	6.734
	200–300	9.429	6.452	0.684	0.156	0.170	0.675	0.830	−0.379	−0.412	0.327	−1.259
	300–400	3.996	1.935	0.484	0.110	0.168	0.722	0.832	−0.725	−0.746	0.583	−1.280
	400–500	2.105	0.000	0.000	0.000	0.000	1.000	1.000	0.000	0.000	0.000	0.000
	> 500	2.813	1.935	0.688	0.157	0.166	0.678	0.834	−0.374	−0.383	0.583	−0.657
Plan curvature	< −1.17	2.029	1.935	0.954	0.224	0.242	0.534	0.758	−0.047	−0.048	0.583	−0.083
	−1.17–−0.32	10.521	7.097	0.675	0.159	0.251	0.590	0.749	−0.394	−0.431	0.313	−1.379
	−0.32–0.45	75.953	71.613	0.943	0.222	0.286	0.493	0.714	−0.059	−0.225	0.178	−1.262
	> 0.45	11.497	19.355	1.683	0.396	0.221	0.384	0.779	0.521	0.614	0.203	3.020
Profile curvature	< −0.65	6.485	9.677	1.492	0.255	0.223	0.522	0.777	0.400	0.435	0.272	1.601
	−0.65–0.21	71.183	56.774	0.798	0.136	0.346	0.518	0.654	−0.226	−0.632	0.162	−3.896
	0.21–1.15	19.352	27.097	1.400	0.239	0.209	0.552	0.791	0.337	0.438	0.181	2.421
	> 1.15	2.980	6.452	2.165	0.370	0.222	0.408	0.778	0.772	0.809	0.327	2.474
SPI	<1	11.943	1.935	0.162	0.049	0.285	0.666	0.715	−1.820	−1.927	0.583	−3.306
	1–4	22.502	18.710	0.831	0.253	0.268	0.479	0.732	−0.185	−0.232	0.206	−1.128
	4–9	20.216	20.000	0.989	0.301	0.257	0.443	0.743	−0.011	−0.013	0.201	−0.067
	>9	45.339	59.355	1.309	0.398	0.190	0.412	0.810	0.269	0.566	0.164	3.459
STI	<1	31.071	9.677	0.311	0.071	0.324	0.604	0.676	−1.166	−1.437	0.272	−5.289
	1–4	27.492	29.677	1.079	0.247	0.240	0.513	0.760	0.076	0.107	0.176	0.609
	4–10	19.692	38.065	1.933	0.443	0.191	0.366	0.809	0.659	0.919	0.165	5.554
	>10	21.745	22.581	1.038	0.238	0.245	0.517	0.755	0.038	0.048	0.192	0.252
TWI	<5	16.680	25.806	1.547	0.429	0.226	0.345	0.774	0.436	0.552	0.184	3.009
	5–7	45.828	57.419	1.253	0.347	0.200	0.453	0.800	0.225	0.466	0.162	2.870
	7–9	23.431	13.548	0.578	0.160	0.287	0.553	0.713	−0.548	−0.669	0.235	−2.851
	>9	14.061	3.226	0.229	0.064	0.286	0.650	0.714	−1.472	−1.591	0.455	−3.500
Distance to rivers (m)	<200	27.491	52.903	1.924	0.433	0.109	0.457	0.891	0.655	1.086	0.161	6.750
	200–400	23.259	31.613	1.359	0.306	0.150	0.544	0.850	0.307	0.422	0.173	2.444
	400–600	19.284	7.742	0.401	0.090	0.193	0.717	0.807	−0.913	−1.046	0.301	−3.481
	600–800	14.429	4.516	0.313	0.070	0.188	0.741	0.812	−1.162	−1.271	0.387	−3.287
	800–1000	9.075	1.290	0.142	0.032	0.183	0.785	0.817	−1.951	−2.033	0.712	−2.856
	>1000	6.461	1.935	0.299	0.067	0.177	0.756	0.823	−1.205	−1.253	0.583	−2.149
Distance to roads (m)	<200	13.245	38.065	2.874	0.420	0.117	0.463	0.883	1.056	1.393	0.165	8.419
	200–400	12.114	7.097	0.586	0.086	0.173	0.741	0.827	−0.535	−0.590	0.313	−1.887
	400–600	11.063	7.097	0.642	0.094	0.171	0.735	0.829	−0.444	−0.488	0.313	−1.559
	600–800	10.253	11.613	1.133	0.166	0.161	0.673	0.839	0.125	0.140	0.251	0.558
	800–1000	9.653	9.677	1.002	0.147	0.164	0.690	0.836	0.003	0.003	0.272	0.010
	>1000	43.673	26.452	0.606	0.089	0.214	0.698	0.786	−0.501	−0.768	0.182	−4.218
Distance to faults (m)	< 1000	13.359	16.774	1.256	0.178	0.157	0.665	0.843	0.228	0.268	0.215	1.246
	1000–2000	11.237	15.484	1.378	0.196	0.156	0.649	0.844	0.321	0.370	0.222	1.665
	2000–3000	10.227	14.839	1.451	0.206	0.155	0.639	0.845	0.372	0.425	0.226	1.881
	3000–4000	9.765	9.032	0.925	0.131	0.165	0.704	0.835	−0.078	−0.086	0.280	−0.307
	4000–5000	9.060	12.258	1.353	0.192	0.158	0.650	0.842	0.302	0.338	0.245	1.381
	>5000	46.353	31.613	0.682	0.097	0.209	0.695	0.791	−0.383	−0.626	0.173	−3.621
NDVI	<0.10	35.566	3.871	0.109	0.010	0.289	0.702	0.711	−2.218	−2.618	0.416	−6.287
	0.10–0.20	22.175	16.129	0.727	0.065	0.209	0.727	0.791	−0.318	−0.393	0.218	−1.800
	0.20–0.30	20.516	17.419	0.849	0.076	0.201	0.723	0.799	−0.164	−0.202	0.212	−0.953
	0.30–0.40	17.042	24.516	1.439	0.128	0.176	0.696	0.824	0.364	0.458	0.187	2.453
	>0.40	4.701	38.065	8.097	0.722	0.126	0.153	0.874	2.092	2.523	0.165	15.248
Land use	Bare	0.655	0.000	0.000	0.000	0.000	1.000	1.000	0.000	0.000	0.000	0.000

Table 2 (continued)

Factors	Classes	Percentage of domain (%)	Percentage of landslide (%)	FR	Bel	Dis	Unc	Pls	SI	C	*S*(*C*)	*C*/*S*(*C*)
	Farmland	0.663	1.935	2.919	0.470	0.162	0.369	0.838	1.072	1.085	0.583	1.861
	Forest	28.806	47.742	1.657	0.267	0.120	0.613	0.880	0.505	0.815	0.161	5.065
	Grass	18.521	18.710	1.010	0.162	0.163	0.674	0.837	0.010	0.012	0.206	0.061
	Residential	50.156	31.613	0.630	0.101	0.225	0.674	0.775	−0.462	−0.778	0.173	−4.503
	Water	1.200	0.000	0.000	0.000	0.000	1.000	1.000	0.000	0.000	0.000	0.000
Lithology	A	8.916	18.065	2.026	0.176	0.089	0.735	0.911	0.706	0.812	0.209	3.889
	B	1.154	1.935	1.677	0.146	0.098	0.756	0.902	0.517	0.525	0.583	0.901
	C	5.998	3.226	0.538	0.047	0.102	0.852	0.898	−0.620	−0.649	0.455	−1.428
	D	49.159	34.194	0.696	0.061	0.128	0.812	0.872	−0.363	−0.621	0.169	−3.668
	E	0.348	0.000	0.000	0.000	0.000	1.000	1.000	0.000	0.000	0.000	0.000
	F	10.174	12.258	1.205	0.105	0.096	0.799	0.904	0.186	0.210	0.245	0.857
	G	8.672	13.548	1.562	0.136	0.093	0.771	0.907	0.446	0.501	0.235	2.135
	H	7.245	0.645	0.089	0.008	0.106	0.887	0.894	−2.419	−2.487	1.003	−2.479
	I	5.986	12.258	2.048	0.178	0.092	0.730	0.908	0.717	0.786	0.245	3.209
	J	2.348	3.871	1.649	0.143	0.097	0.759	0.903	0.500	0.516	0.416	1.239
Rainfall (mm/yr)	765.3–957.4	5.295	9.032	1.706	0.304	0.191	0.505	0.809	0.534	0.574	0.280	2.050
	957.4–1041.7	23.350	37.419	1.603	0.286	0.163	0.552	0.837	0.472	0.674	0.166	4.063
	1041.7–1109.6	30.788	22.581	0.733	0.131	0.223	0.646	0.777	−0.310	−0.422	0.192	−2.197
	1109.6–1189.3	22.409	12.903	0.576	0.103	0.224	0.674	0.776	−0.552	−0.668	0.240	−2.786
	1189.3–1362.6	18.158	18.065	0.995	0.177	0.199	0.623	0.801	−0.005	−0.006	0.209	−0.030

$$AUC = \frac{\sum TP + \sum TN}{P + N} \tag{19}$$

where TP is the number of landslides classified correctly, TN is the number of landslides classified incorrectly, P is the total number of landslides, and N is the total number of non-landslides.

The success rate and prediction rate curves of the landslide susceptibility maps were also used in this study. The curves were obtained by plotting the cumulative percentage of landslide susceptibility maps on the x-axis and the cumulative percentage of landslide pixels on the y-axis. The areas under the curves of the success rate (AUC_T) and the prediction rate (AUC_P) were used to reflect the prediction capability of the landslide susceptibility maps.

Results

Analyses of landslide conditioning factors

Multicollinearity analysis was calculated with the training dataset using IBM SPSS Statistics software. The results, shown in Tables 2 and 3, indicate that there were no multicollinearities among the 15 landslide conditioning factors.

In addition to the multicollinearity analysis, the predictive capabilities of the landslide conditioning factors were assessed by applying the KLR model with the RBF kernel function. The results of the most effective conditioning factors of the different ensemble models are shown in Table 4. The results indicate that all factors contributed to the models. Altitude, with the highest average merit (AM) in three ensemble models, was found to be the most important factor, followed in descending order by distance to rivers, distance to roads, STI, TWI, lithology, NDVI, distance to faults, SPI, slope angle, rainfall, aspect, land use, and plan and profile curvatures, respectively. Some factors including rainfall, aspect, land use, and plan and profile curvatures made only small contributions to the landslide modeling. However, as all the AMs had positive values, all 15 conditioning factors were considered in constructing the landslide susceptibility maps.

Ensemble of EBF and KLR models

In this study, the parameters of the EBF method (i.e., Bel, Dis, Unc, and Pls) were obtained using the equations introduced earlier (section "Evidential belief function (EBF)") for each class of conditioning factors. These parameters were computed based on the ratio between the number of landslides per class and the area of each class. The results of the EBF method can be seen in Table 2.

All Pls weights of the conditioning factors were used as input datasets for the EBF and EBF-KLR methods. For each pixel of the study area, the probability of landslide occurrence (PLO) using a linear logistic regression function (Eq. 12) was computed. The PLOs were reclassified based on the area

Table 3 Multicollinearity analysis

Number	Factors	EBF		SI		WOE	
		TOL	VIF	TOL	VIF	TOL	VIF
1	Slope angle	0.639	1.564	0.664	1.506	0.546	1.830
2	Slope aspect	0.951	1.051	0.953	1.049	0.943	1.061
3	Altitude	0.719	1.391	0.748	1.337	0.712	1.405
4	Plan curvature	0.789	1.268	0.821	1.218	0.828	1.208
5	Profile curvature	0.841	1.189	0.848	1.179	0.825	1.212
6	SPI	0.484	2.068	0.536	1.864	0.413	2.419
7	STI	0.411	2.432	0.395	2.529	0.398	2.511
8	TWI	0.642	1.558	0.657	1.523	0.695	1.439
9	Distance to rivers	0.880	1.136	0.881	1.135	0.875	1.143
10	Distance to roads	0.916	1.092	0.921	1.085	0.925	1.081
11	Distance to faults	0.839	1.191	0.818	1.223	0.810	1.235
12	NDVI	0.811	1.233	0.554	1.805	0.586	1.707
13	Land use	0.919	1.088	0.655	1.526	0.655	1.526
14	Lithology	0.686	1.457	0.647	1.547	0.927	1.078
15	Rainfall	0.914	1.094	0.926	1.080	0.922	1.085

percentage method to construct the landslide susceptibility map. The landslide susceptibility maps based on the EBF and the ensemble of EBF and KLR are shown in Fig. 5a and b, respectively.

Ensemble of SI and KLR models

Similar to the process of combination of the EBF and KLR methods, the SI was computed for each class of conditioning factors. Then, the SIs were assigned as weights to each class. Eventually, each conditioning factor was reclassified based on its SI and was determined as an input for overlaying with the landslides to extract the dataset for the KLR algorithm. The results of the SI are displayed in Table 2.

All conditioning factors were reclassified based on their SI and then applied as input datasets for the SI and SI-KLR methods. The PLOs were also reclassified based on the area percentage method to construct the landslide susceptibility map. The landslide susceptibility maps based on the SI and SI-KLR models are shown in Fig. 5c and d, respectively.

Ensemble of WoE and KLR models

In the WoE-KLR ensemble model, the parameters C, S (C), and C/S (C) were calculated first based on their function, as described in section "Weights of evidence (WoE)". The C/S (C) weights were transferred to each class of conditioning factors. Then, each factor was reclassified and overlaid with the landslide locations to construct a database for computing the PLOs using the KLR algorithm.

Similar to the EBF and SI models, the WoE model was used to establish the spatial relationship between each conditioning factor and the landslide locations. The results of SI are presented in Table 2. Based on the C/S(C) of the WoE model, all conditioning factors were reclassified and applied as input datasets for the WoE and WoE-KLR methods. The PLOs were also

Table 4 Predictive capabilities of conditioning factors using KLR model

Number	Factors	EBF-KLR		SI-KLR		WOE-KLR	
		AM	S.D	AM	S.D	AM	S.D
1	Altitude	0.155	±0.009	0.152	±0.011	0.155	±0.010
2	Distance to rivers	0.142	±0.008	0.142	±0.008	0.135	±0.011
3	Distance to roads	0.135	±0.010	0.135	±0.011	0.130	±0.015
4	STI	0.135	±0.011	0.128	±0.012	0.128	±0.012
5	TWI	0.116	±0.017	0.126	±0.009	0.118	±0.020
6	Lithology	0.116	±0.006	0.116	±0.007	0.116	±0.010
7	NDVI	0.116	±0.009	0.116	±0.009	0.116	±0.010
8	Distance to faults	0.105	±0.012	0.102	±0.014	0.106	±0.010
9	SPI	0.106	±0.010	0.100	±0.008	0.094	±0.010
10	Slope	0.103	±0.007	0.087	±0.006	0.080	±0.016
11	Rainfall	0.069	±0.012	0.081	±0.007	0.062	±0.007
12	Aspect	0.067	±0.007	0.078	±0.008	0.061	±0.013
13	Land use	0.045	±0.013	0.041	±0.014	0.044	±0.014
14	Plan curvature	0.033	±0.012	0.033	±0.012	0.031	±0.009
15	Profile curvature	0.023	±0.022	0.025	±0.021	0.019	±0.028

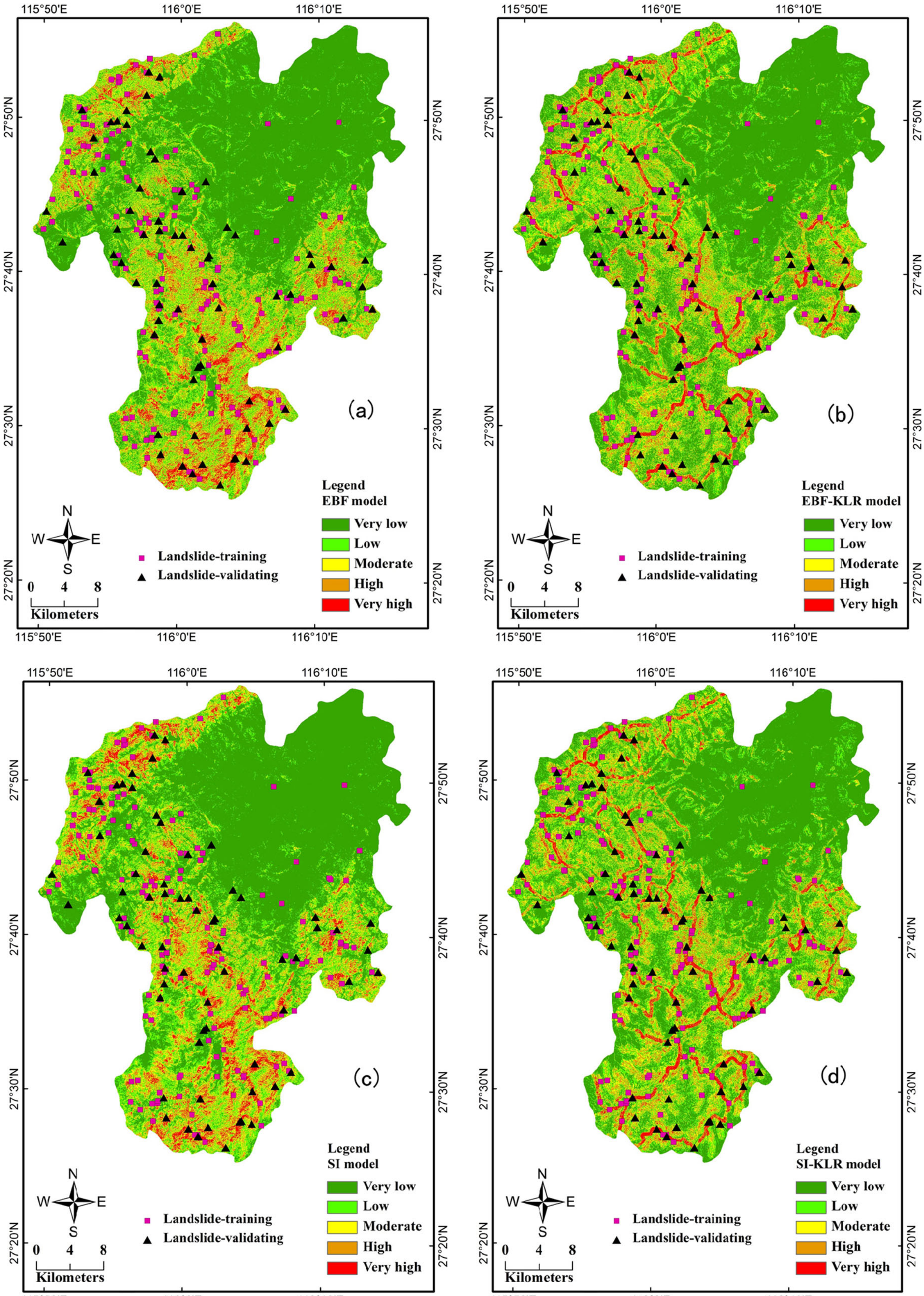

Fig. 5 Landslide susceptibility maps by (**a**) EBF, (**b**) EBF-KLR, (**c**) SI, (**d**) SI-KLR, (**e**) WoE, (**f**) WoE-KLR models

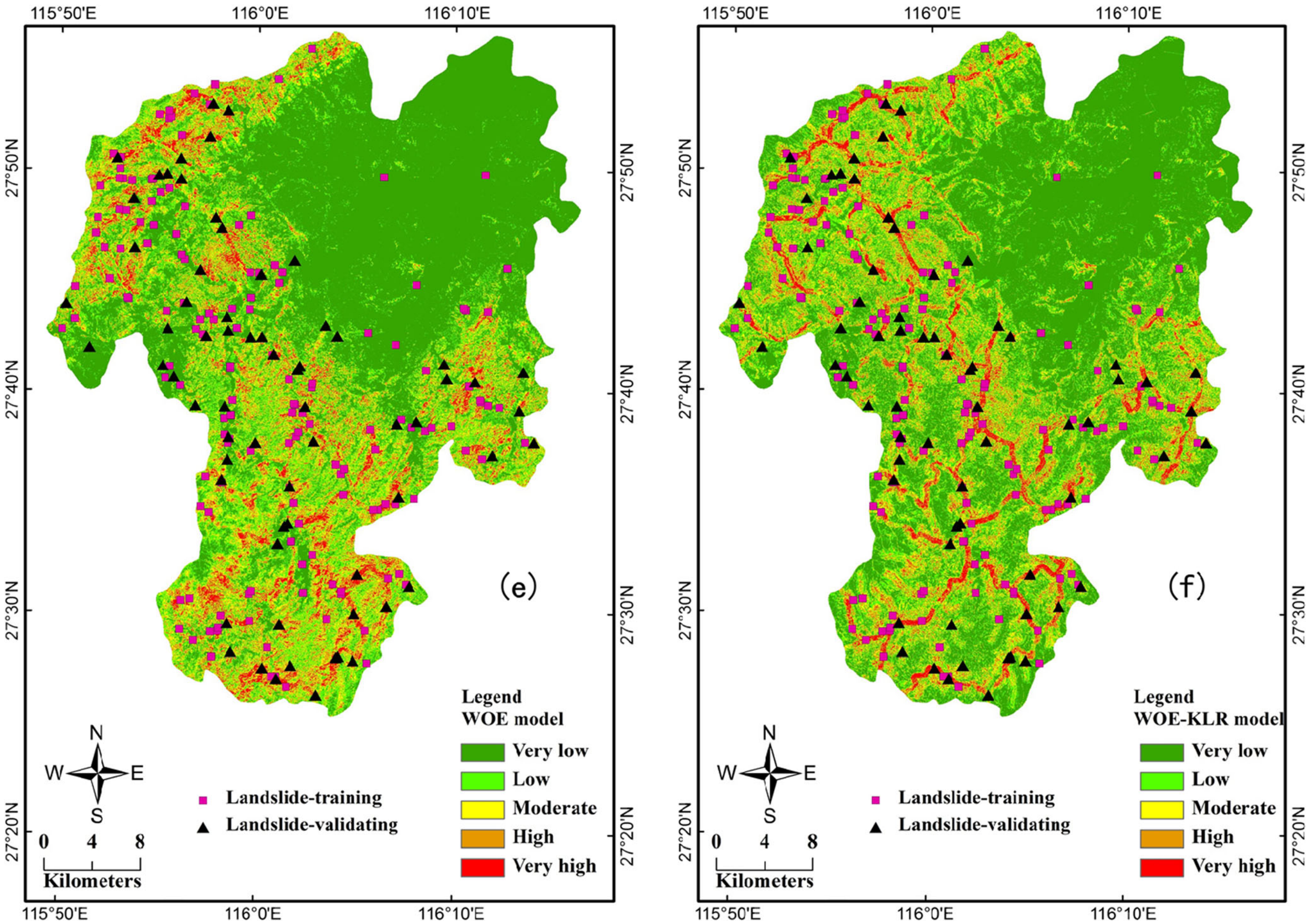

Fig. 5 (continued)

reclassified according to the area percentage method to construct the landslide susceptibility map. The landslide susceptibility maps based on the WoE and WoE-KLR models are shown in Fig. 5e and f, respectively.

In order to present a better comparison of landslide susceptibility maps, the five landslide susceptibility classes were determined as very high (5%), high (10%), moderate (15%), low (20%), and very low (50%) for the six landslide susceptibility maps.

Ensemble models' performance and comparison

The AUC curve with the training dataset was used to assess the performances of the three ensemble models, as shown in Table 5 and Fig. 6a. The results indicate that all ensemble models have high prediction accuracy according to the AUC values. Additionally, the EBF-KLR ensemble model has the highest AUC value (AUC = 0.814) followed by the SI-KLR ensemble model (AUC = 0.811) and the WoE-KLR ensemble model (AUC = 0.806). The performances of the three ensemble models based on the AUROC with the validation dataset are shown in Table 6 and Fig. 6b. The results indicate the EBF-KLR ensemble model (AUC = 0.753) outperformed the SI-KLR ensemble model (AUC = 0.752) and the WoE-KLR ensemble model (AUC = 0.744). These findings suggest that although all landslide susceptibility ensemble models showed high prediction accuracy, the EBF-KLR ensemble model had the highest prediction capability for landslide susceptibility mapping in the study area.

Table 5 Ensemble models' performance using training dataset

Model	AUC	SE	95% CI
EBF-KLR	0.814	0.0238	0.766 to 0.856
SI-KLR	0.811	0.0242	0.763 to 0.853
WoE-KLR	0.806	0.0244	0.758 to 0.849

Validation of landslide susceptibility maps

The validation of the six landslide susceptibility maps produced by the three bivariate models and the three

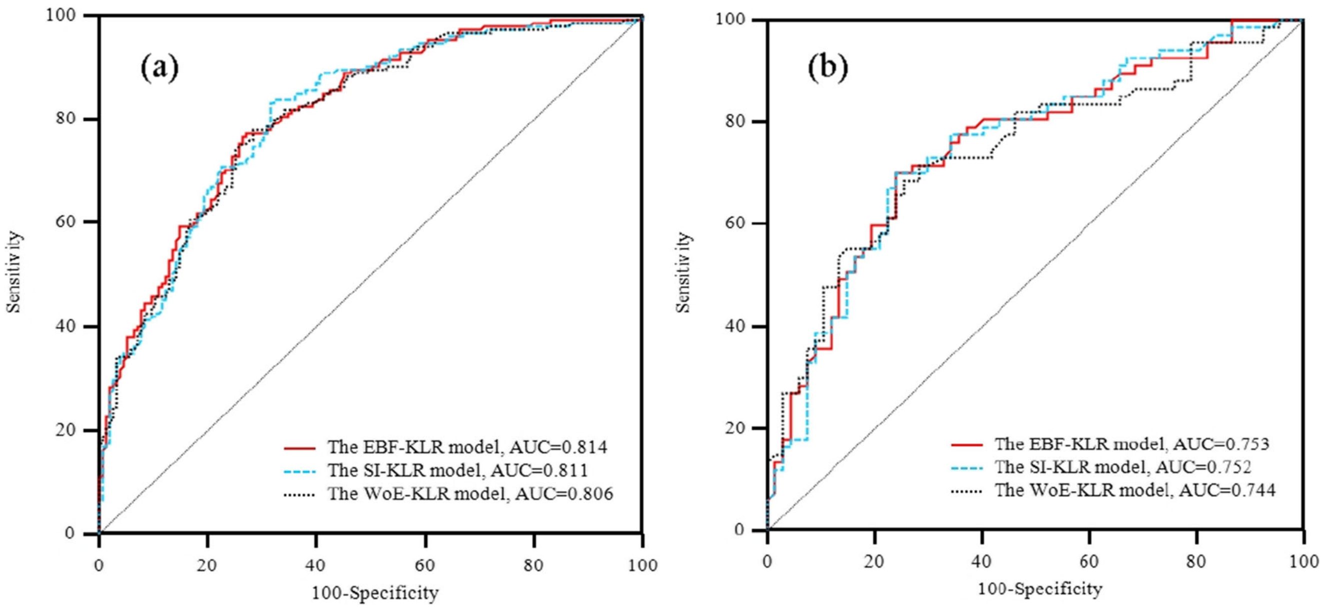

Fig. 6 Comparison of the three ensemble landslide models using the AUROC curve with **a** the training dataset and **b** the validation dataset

ensemble models were assessed based on the spatial cross-validation procedure mentioned in section "Model performance and validation of landslide susceptibility maps". The corresponding AUC_T and AUC_P curves are shown in Figs. 7 and 8 and validation of the landslide susceptibility maps is presented in Table 7. For the training dataset, the EBF-KLR model had the highest prediction capability (0.8511), followed in descending order by the SI-KLR model (0.8505), WoE-KLR model (0.8397), EBF model (0.7978), SI model (0.7951), and WoE model (0.7825). For the validation dataset, the EBF-KLR model had the highest prediction capability (0.7615), followed in descending order by the SI-KLR model (0.7595), SI model (0.7503), EBF model (0.7437), WoE-KLR model (0.7286), and WoE model (0.7198). Thus, the results show the ensemble EBF-KLR was the most capable of mapping landslide susceptibility within the study area.

Landslide density (LD) was also calculated to validate the landslide susceptibility maps. The LD is defined as the ratio between the percentages of landslides and the percentages of each susceptible class (Pham et al. 2016); higher susceptible classes should have higher LDs for reliable landslide susceptibility maps. As mentioned above, the area percentages of each susceptible class were defined as very high (5%), high (10%), moderate (15%), low (20%), and very low (50%). Therefore, it is only necessary to calculate the percentages of landslide locations for each class. The results of the LD analysis are shown in Table 8. It can be observed that the very high class has the highest LD values, followed in descending order by the high, moderate, low, and very low classes. The results also show that the ensemble models yielded better performance than the individual bivariate models, and that the EBF-KLR model improved the performance of the bivariate EBF model more significantly than the other two ensemble models.

Table 6 Ensemble models' performance using validating dataset

Model	AUC	SE	95% CI
EBF-KLR	0.753	0.0422	0.671 to 0.824
SI-KLR	0.752	0.0424	0.670 to 0.822
WoE-KLR	0.744	0.0431	0.661 to 0.815

Discussion

Landslide susceptibility describes the probability of landslide occurrence within a particular area, and the correlation between previous landslide locations and possible conditioning factors (Romer and Ferentinou 2016). In previous decades, many methods including traditional statistical models (Ding et al. 2017; Zhang et al. 2016a) and sophisticated machine learning models (Chen et al. 2017g; Pourghasemi and Kerle 2016; Youssef et al. 2016) have been used in conjunction with the development of GIS technology to predict the

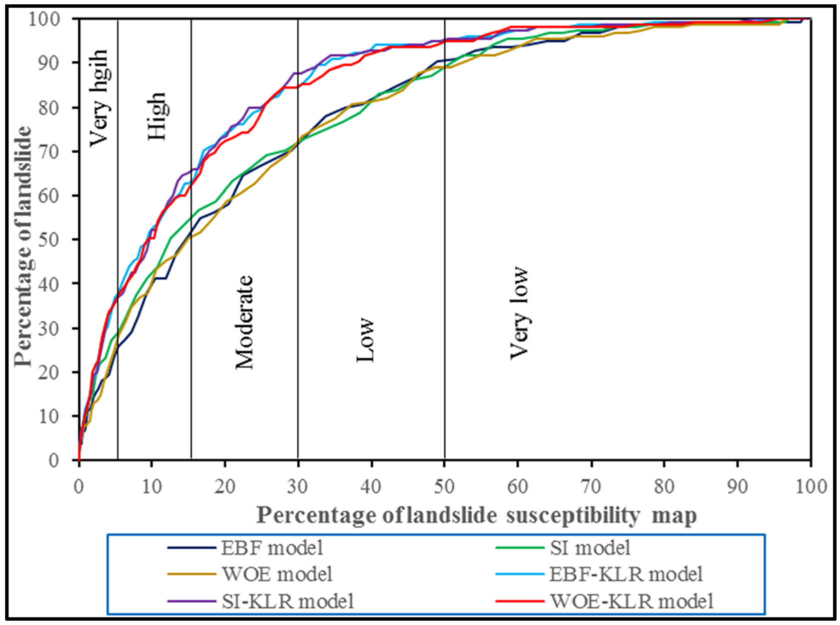

Fig. 7 Model validation with the success rate (AUC_T) curve for the six landslide susceptibility maps

spatial distributions of landslides. However, both bivariate and machine learning approaches have their limitations, which could potentially be eliminated by the use of ensemble models. Therefore, it is necessary to explore and to compare new ensemble methods and techniques in application to landslide modeling. Recently, some ensemble machine learning methods have been applied in landslide susceptibility, for example, Shirzadi et al. (2017) used a Naive Bayes trees (NBT) and random subspace (RS) ensemble method for landslide susceptibility mapping at the Bijar region, Kurdistan province (Iran), and their result showed that NBT-RS significantly improved the performance of the NBT base classifier. Hong et al. (2018) found that J48 Decision Tree with the Rotation Forest model presents the highest prediction capability (AUC =0.855); it improved the performance of the J48 Decision Tree base classifier significantly. Pham et al. (2018) integrated the MultiBoost (MB) ensemble and support vector machine (SVM) for modeling of

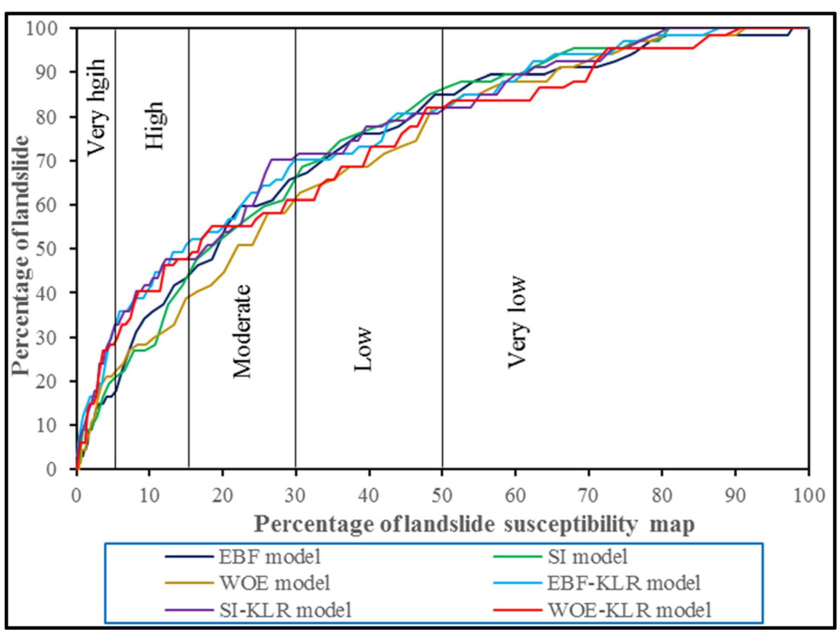

Fig. 8 Model validation with the prediction rate (AUC_P) curve for the six landslide susceptibility maps

Table 7 Validation of landslide susceptibility maps

AUC_T/P	EBF	SI	WoE	EBF-KLR	SI-KLR	WoE-KLR
AUC_T	0.7978	0.7951	0.7825	0.8511	0.8505	0.8397
AUC_P	0.7437	0.7503	0.7198	0.7615	0.7597	0.7286

susceptibility of landslides in the Uttarakhand State, Northern India, and their result showed that the MBSVM outperforms the LR and single SVM models. Though many ensemble methods have been applied in landslide susceptibility, until now, there is still no agreement on which is the best ensemble method in landslide susceptibility mapping. In addition, more experiments are needed to compare different areas to find the difference among each method.

The most important step was to select the landslide conditioning factors because they affect the quality of landslide susceptibility analysis (Irigaray et al. 2007; Romer and Ferentinou 2016). However, there are no standard guidelines regarding the selection of landslide conditioning factors (Tien Bui et al. 2016). This study built a landslide susceptibility model using 15 landslide conditioning factors that included topographical, geological, and environmental factors. Then, TOL and VIF were used to establish the absence of multicollinearity among the 15 landslide conditioning factors (Table 3). Subsequently, the classifier attribute evaluation method (Witten et al. 2011) using the KLR model with the RBF kernel function was used to assess the importance of the variables. The results showed that all 15 conditioning factors had positive predictive capability in the model (Table 4); therefore, they were all used to build landslide susceptibility models.

The goodness-of-fits of three ensemble models were evaluated using ROC and AUC values. The results indicated that all ensemble models had high prediction accuracy based on the AUC values. The EBF-KLR ensemble model had the highest AUC values for both the training (AUC = 0.814) and the validation (AUC = 0.753) datasets, followed in descending order by the SI-KLR ensemble model and the WoE-KLR ensemble model (Tables 5 and 6). However, the results also showed that different conditioning factors had different contributions to the models (Table 4). In general, altitude, distance to rivers, and distance to roads were found to be the most important factors for the three ensemble models. Conversely, the factors of land use, profile curvature, and plan curvature yielded the lowest predictive capabilities for the three ensemble models. The normalized predictive capabilities of the conditioning factors for the three ensemble models were used to visualize the relative importance of the 15 conditioning factors (Fig. 9). It was observed that altitude contributed the highest percentages of 10.573, 10.397, and 11.111% for the EBF-KLR, SI-KLR, and WoE-KLR models, respectively; distance to rivers yielded the second highest contributions of 9.688, 9.713, and 9.677%, respectively, and distance to roads yielded the third highest contributions of 9.209, 9.234, and 9.319%, respectively. In contrast, profile curvature yielded the lowest contributions of 1.569, 1.710, and 1.362%, respectively. Therefore, because of the types of input variables and the models used, it was concluded that landslide conditioning factors tend to have different contributions (Tien Bui et al. 2016). Further studies should be undertaken to explore the optimum method for selecting the optimal factors for both this and similar study areas.

To evaluate and compare the three ensemble models with the three individual bivariate models, this study adopted the methods of the AUC_T and AUC_P curves, and LD analysis. The results suggested the three ensemble models showed higher prediction capabilities for both the training and the validation datasets than each of the three individual bivariate models. The EBF-KLR ensemble exhibited the optimal performance, which could improve the performance of the EBF model

Table 8 Landslide density analysis on landslide susceptibility maps

Class	EBF-KLR		EBF		SI-KLR		SI		WoE-KLR		WoE	
	PLL	LD	PLL	LD	PLL	LD	PLL	LD	PLL	LD	PLL	LD
Very low	5.16	0.10	11.61	0.23	5.16	0.10	12.90	0.26	5.81	0.12	10.97	0.22
Low	10.32	0.52	18.71	0.94	7.74	0.39	16.77	0.84	9.68	0.48	20.00	1.00
Moderate	21.94	1.46	22.58	1.51	22.58	1.51	19.35	1.29	25.16	1.68	22.58	1.51
High	27.74	2.77	26.45	2.65	29.03	2.90	25.81	2.58	24.52	2.45	24.52	2.45
Very high	34.84	6.97	20.65	4.13	35.48	7.10	25.16	5.03	34.84	6.97	21.94	4.39

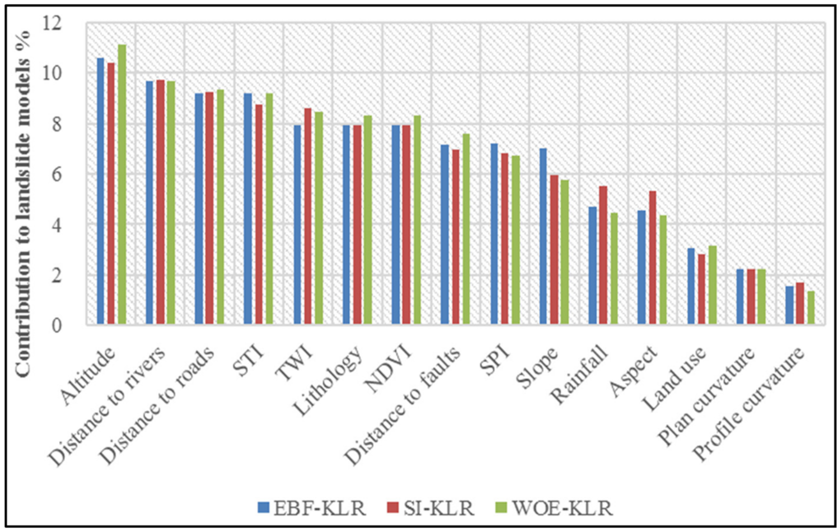

Fig. 9 Relative importance of conditioning factors for different ensemble models

significantly. However, it should be noted that the other two ensembles also yielded reasonable performance.

Conclusions

This study evaluated landslide susceptibility in Chongren County (China) using novel ensembles of bivariate statistical-methods-based (EBF, SI, and WoE) kernel logistic regression machine learning classifiers. A series of conditioning factors (slope angle, slope aspect, altitude, plan curvature, profile curvature, SPI, STI, TWI, distance to rivers, distance to roads, distance to faults, NDVI, land use, lithology, and rainfall) were used as the inputs to the three hybrid models. A landslide inventory comprising 222 landslides was divided randomly into a training set (70%) for evaluation of the landslide susceptibility models and a validation set (30%) for validation of the model procedure.

The results showed that the three hybrid models were successful at identifying landslide-prone areas. The results also showed that the hybrid models could improve the predictive capability of the bivariate models, and that the EBF-KLR hybrid model yielded the highest predictive capability in landslide susceptibility assessment.

In conclusion, the landslide susceptibility maps produced in the present study may be useful for land use planning and decision making in areas prone to landslides. Moreover, this study also demonstrated the superiority of hybrid models in landslide susceptibility modeling.

Acknowledgments This research was supported by the International Partnership Program of Chinese Academy of Sciences (Grant No. 115242KYSB20170022), the National Natural Science Foundation of China (Grant No. 41807192), China Postdoctoral Science Foundation (Grant No. 2018 T111084, 2017 M613168), Project funded by Shaanxi Province Postdoctoral Science Foundation (Grant No. 2017BSHYDZZ07), and the Open Fund of Shandong Provincial Key Laboratory of Depositional Mineralization & Sedimentary Minerals (Grant No. DMSM2017029). We thank James Buxton MSc from Edanz Group (www.edanzediting.com./ac) for editing a draft of this manuscript.

References

Agterberg FP (1989) Computer programs for mineral exploration. Science 245:76–81

Althuwaynee OF, Pradhan B, Park HJ, Lee JH (2014) A novel ensemble decision tree-based CHi-squared automatic interaction detection (CHAID) and multivariate logistic regression models in landslide susceptibility mapping. Landslides 11:1063–1078

Althuwaynee OF, Pradhan B, Ahmad N (2015) Estimation of rainfall threshold and its use in landslide hazard mapping of Kuala Lumpur metropolitan and surrounding areas. Landslides 12:861–875

Benediktsson JA, Swain PH, Ersoy OK (1989) Neural network approaches versus statistical methods in classification of multisource remote sensing data, geoscience and remote sensing symposium. Igarss'89. Canadian symposium on remote sensing, pp 489–492

Beullens J, Velde DVD, Nyssen J (2014) Impact of slope aspect on hydrological rainfall and on the magnitude of rill erosion in Belgium and northern France. Catena 114:129–139

Bonham-Carter GF (1994) Geographic information systems for geoscientists-modeling with GIS. Computer methods in the geoscientists 13:398

Broeckx J, Vanmaercke M, Duchateau R, Poesen J (2018) A data-based landslide susceptibility map of Africa. Earth Sci Rev 185:102–121

Cawley GC, Talbot NL (2005) The evidence framework applied to sparse kernel logistic regression. Neurocomputing 64:119–135

Chen X-L, Liu C-G, Chang Z-F, Zhou Q (2016) The relationship between the slope angle and the landslide size derived from limit equilibrium simulations. Geomorphology 253:547–550

Chen W, Panahi M, Pourghasemi HR (2017a) Performance evaluation of GIS-based new ensemble data mining techniques of adaptive neuro-fuzzy inference system (ANFIS) with genetic algorithm (GA), differential evolution (DE), and particle swarm optimization (PSO) for landslide spatial modelling. CATENA 157:310–324

Chen W, Pourghasemi HR, Kornejady A, Zhang N (2017b) Landslide spatial modeling: introducing new ensembles of ANN, MaxEnt, and SVM machine learning techniques. Geoderma 305:314–327

Chen W, Pourghasemi HR, Naghibi SA (2017c) A comparative study of landslide susceptibility maps produced using support vector machine with different kernel functions and entropy data mining models in China. Bull Eng Geol Environ. https://doi.org/10.1007/s10064-017-1010-y

Chen W, Pourghasemi HR, Naghibi SA (2017d) Prioritization of landslide conditioning factors and its spatial modeling in Shangnan County, China using GIS-based data mining algorithms. Bull Eng Geol Environ. https://doi.org/10.1007/s10064-017-1004-9

Chen W et al (2017e) A novel hybrid artificial intelligence approach based on the rotation forest ensemble and naïve Bayes tree classifiers for a landslide susceptibility assessment in Langao County, China. Geomatics, Nat Hazards Risk 8:1955–1977

Chen W et al (2017f) GIS-based landslide susceptibility modelling: a comparative assessment of kernel logistic regression, Naïve-Bayes tree, and alternating decision tree models. Geomat Nat Haz Risk 8: 950–973

Chen W et al (2017g) A comparative study of logistic model tree, random forest, and classification and regression tree models for spatial prediction of landslide susceptibility. CATENA 151:147–160

Chung C-JF, Fabbri AG (2003) Validation of spatial prediction models for landslide hazard mapping. Nat Hazards 30:451–472

Dempster AP (1967) Upper and lower probabilities induced by a multivalued mapping. Ann Math Stat 38:325–339

Ding Q, Chen W, Hong H (2017) Application of frequency ratio, weights of evidence and evidential belief function models in landslide susceptibility mapping. Geocarto International 32:619–639

Domínguez-Cuesta MJ, Jiménez-Sánchez M, Berrezueta E (2007) Landslides in the central coalfield (Cantabrian Mountains, NW Spain): geomorphological features, conditioning factors and methodological implications in susceptibility assessment. Geomorphology 89:358–369

ESRI (2014) ArcGIS desktop: release 10.2. Environmental Systems Research Institute, Redlands

Galli M, Ardizzone F, Cardinali M, Guzzetti F, Reichenbach P (2008) Comparing landslide inventory maps. Geomorphology 94:268–289

Guzzetti F et al (2012) Landslide inventory maps: new tools for an old problem. Earth Sci Rev 112:42–66

Harp EL, Keefer DK, Sato HP, Yagi H (2011) Landslide inventories: the essential part of seismic landslide hazard analyses. Eng Geol 122:9–21

Hong H, Pradhan B, Xu C, Tien Bui D (2015) Spatial prediction of landslide hazard at the Yihuang area (China) using two-class kernel logistic regression, alternating decision tree and support vector machines. Catena 133:266–281

Hong H, Pourghasemi HR, Pourtaghi ZS (2016) Landslide susceptibility assessment in Lianhua County (China): a comparison between a random forest data mining technique and bivariate and multivariate statistical models. Geomorphology 259:105–118

Hong H et al (2017) Rainfall-induced landslide susceptibility assessment at the Chongren area (China) using frequency ratio, certainty factor, and index of entropy. Geocarto International 32:139–154

Hong H et al (2018) Landslide susceptibility mapping using J48 decision tree with AdaBoost, bagging and rotation Forest ensembles in the Guangchang area (China). Catena 163:399–413

Irigaray C, Fernández T, Hamdouni RE, Chacón J (2007) Evaluation and validation of landslide-susceptibility maps obtained by a GIS matrix method: examples from the Betic cordillera (southern Spain). Nat Hazards 41:61–79

Iwahashi J, Watanabe S, Furuya T (2003) Mean slope-angle frequency distribution and size frequency distribution of landslide masses in Higashikubiki area, Japan. Geomorphology 50:349–364

Jebur MN, Pradhan B, Tehrany MS (2014) Optimization of landslide conditioning factors using very high-resolution airborne laser scanning (LiDAR) data at catchment scale. Remote Sens Environ 152: 150–165

Jiménez Sánchez M, Farias P, Rodríguez A, Menéndez Duarte RA (1999) Landslide development in a coastal valley in northern Spain: conditioning factors and temporal occurrence. Geomorphology 30:115–123

Jonathan B, Marko H, Robert B, Brian H (2006) Influence of slope and aspect on long-term vegetation change in British chalk grasslands. J Ecol 94:355–368

Kimeldorf G, Wahba G (1971) Some results on Tchebycheffian spline functions. J Math Anal Appl 33:82–95

Kritikos T, Davies T (2015) Assessment of rainfall-generated shallow landslide/debris-flow susceptibility and runout using a GIS-based approach: application to western southern Alps of New Zealand. Landslides 12:1051–1075

Kumar R, Anbalagan R (2016) Landslide susceptibility mapping using analytical hierarchy process (AHP) in Tehri reservoir rim region, Uttarakhand. J Geol Soc India 87:271–286

Lin H-T, Lin C-J (2003) A study on sigmoid kernels for SVM and the training of non-PSD kernels by SMO-type methods. Neural Comput 3:1–32

Ma T, Li C, Lu Z, Bao Q (2015) Rainfall intensity–duration thresholds for the initiation of landslides in Zhejiang Province, China. Geomorphology 245:193–206

Mercer J (1909) Functions of positive and negative type, and their connection with the theory of integral equations. Philosophical Transactions of the Royal Society of London. Series A, Containing Papers of a Mathematical or Physical Character 209: 415–446

Mogaji K, Omosuyi G, Adelusi A, Lim H (2016) Application of GIS-based evidential belief function model to regional groundwater recharge potential zones mapping in Hardrock geologic terrain. Environmental Processes 3:93–123

Moosavi V, Talebi A, Shirmohammadi B (2014) Producing a landslide inventory map using pixel-based and object-oriented approaches optimized by Taguchi method. Geomorphology 204:646–656

Nasiri Aghdam I, Varzandeh MHM, Pradhan B (2016) Landslide susceptibility mapping using an ensemble statistical index (Wi) and adaptive neuro-fuzzy inference system (ANFIS) model at Alborz Mountains (Iran). Environ Earth Sci 75:1–20

O'brien RM (2007) A caution regarding rules of thumb for variance inflation factors. Qual Quant 41:673–690

Pham BT, Tien Bui D, Pourghasemi HR, Indra P, Dholakia MB (2015) Landslide susceptibility assessment in the Uttarakhand area (India) using GIS: a comparison study of prediction capability of naïve bayes, multilayer perceptron neural networks, and functional trees methods. Theor Appl Climatol 128:255–273

Pham BT, Tien Bui D, Prakash I, Dholakia MB (2016) Rotation forest fuzzy rule-based classifier ensemble for spatial prediction of landslides using GIS. Nat Hazards 83:97–127

Pham BT, Jaafari A, Prakash I, Bui DT (2018) A novel hybrid intelligent model of support vector machines and the MultiBoost ensemble for landslide susceptibility modeling. Bull Eng Geol Environ. https://doi.org/10.1007/s10064-018-1281-y

Pourghasemi HR (2014) Landslide hazard prediction using data mining methods in the North of Tehran City. Dissertation, Tarbiat Modares University, p 143 (In Persian)

Pourghasemi HR (2016) GIS-based forest fire susceptibility mapping in Iran: a comparison between evidential belief function and binary logistic regression models. Scand J For Res 31:80–98

Pourghasemi HR, Kerle N (2016) Random forests and evidential belief function-based landslide susceptibility assessment in Western Mazandaran Province, Iran. Environ Earth Sci 75:1–17

Pourghasemi HR, Rahmati O (2018) Prediction of the landslide susceptibility: which algorithm, which precision? CATENA 162:177–192
Pourghasemi HR, Rossi M (2016) Landslide susceptibility modeling in a landslide prone area in Mazandaran Province, north of Iran: a comparison between GLM, GAM, MARS, and M-AHP methods. Theor Appl Climatol. https://doi.org/10.1007/s00704-016-1919-2
Pradhan B (2013) A comparative study on the predictive ability of the decision tree, support vector machine and neuro-fuzzy models in landslide susceptibility mapping using GIS. Comput Geosci 51: 350–365
Pradhan B, Abokharima MH, Jebur MN, Tehrany MS (2014) Land subsidence susceptibility mapping at Kinta Valley (Malaysia) using the evidential belief function model in GIS. Nat Hazards 73:1019–1042
Rahmati O, Pourghasemi HR, Zeinivand H (2016) Flood susceptibility mapping using frequency ratio and weights-of-evidence models in the Golastan Province, Iran. Geocarto International 31:42–70
Raja NB, Çiçek I, Türkoğlu N, Aydin O, Kawasaki A (2017) Landslide susceptibility mapping of the Sera River basin using logistic regression model. Nat Hazards 85:1323–1346
Regmi AD et al (2014) Application of frequency ratio, statistical index, and weights-of-evidence models and their comparison in landslide susceptibility mapping in Central Nepal Himalaya. Arab J Geosci 7: 725–742
Reichenbach P, Rossi M, Malamud BD, Mihir M, Guzzetti F (2018) A review of statistically-based landslide susceptibility models. Earth Sci Rev 180:60–91
Romer C, Ferentinou M (2016) Shallow landslide susceptibility assessment in a semiarid environment — a quaternary catchment of KwaZulu-Natal, South Africa. Eng Geol 201:29–44
Schölkopf B, Herbrich R, Smola AJ (2001) A generalized representer theorem, computational learning theory. Springer, Heidelberg, pp 416–426
Shafer G (1976) A mathematical theory of evidence. Technometrics 20: 242
Shirzadi A et al (2017) Shallow landslide susceptibility assessment using a novel hybrid intelligence approach. Environ Earth Sci 76:60
Tahmassebipoor N, Rahmati O, Noormohamadi F, Lee S (2016) Spatial analysis of groundwater potential using weights-of-evidence and evidential belief function models and remote sensing. Arab J Geosci 9:1–18
Tehrany MS, Pradhan B, Jebur MN (2014) Flood susceptibility mapping using a novel ensemble weights-of-evidence and support vector machine models in GIS. J Hydrol 512:332–343
Tien Bui D, Pradhan B, Lofman O, Revhaug I, Dick OB (2012) Landslide susceptibility mapping at Hoa Binh province (Vietnam) using an adaptive neuro-fuzzy inference system and GIS. Comput Geosci 45:199–211
Tien Bui D et al (2015) A novel hybrid evidential belief function-based fuzzy logic model in spatial prediction of rainfall-induced shallow landslides in the Lang Son city area (Vietnam). Geomatics, Natural Hazards and Risk 6:243–271
Tien Bui D, Tuan TA, Klempe H, Pradhan B, Revhaug I (2016) Spatial prediction models for shallow landslide hazards: a comparative assessment of the efficacy of support vector machines, artificial neural networks, kernel logistic regression, and logistic model tree. Landslides 13:361–378
Tsangaratos P, Ilia I, Hong H, Chen W, Xu C (2017) Applying information theory and GIS-based quantitative methods to produce landslide susceptibility maps in Nancheng County, China. Landslides 14: 1091–1111
van Westen C (1997) Statistical landslide hazard analysis. ILWIS 2.1 for Windows application guide, pp 73–84
van Westen CJ, Rengers N, Soeters R (2003) Use of geomorphological information in indirect landslide susceptibility assessment. Nat Hazards 30:399–419
Wang L-J, Guo M, Sawada K, Lin J, Zhang J (2016) A comparative study of landslide susceptibility maps using logistic regression, frequency ratio, decision tree, weights of evidence and artificial neural network. Geosci J 20:117–136
Witten IH, Frank E, Mark AH (2011) Data mining: practical machine learning tools and techniques, 3rd edn. Morgan Kaufmann, Burlington
Yilmaz I (2010) Comparison of landslide susceptibility mapping methodologies for Koyulhisar, Turkey: conditional probability, logistic regression, artificial neural networks, and support vector machine. Environ Earth Sci 61:821–836
Youssef AM, Al-Kathery M, Pradhan B (2015) Landslide susceptibility mapping at Al-hasher area, Jizan (Saudi Arabia) using GIS-based frequency ratio and index of entropy models. Geosci J 19:113–134
Youssef AM, Pourghasemi HR, Pourtaghi ZS, Al-Katheeri MM (2016) Landslide susceptibility mapping using random forest, boosted regression tree, classification and regression tree, and general linear models and comparison of their performance at Wadi Tayyah Basin, Asir region, Saudi Arabia. Landslides 13:839–856
Yuan RM et al (2013) Density distribution of landslides triggered by the 2008 Wenchuan earthquake and their relationships to peak ground acceleration. Bull Seismol Soc Am 103:2344–2355
Yuan R-m, Tang C-L, Deng Q-h (2015) Effect of the acceleration component normal to the sliding surface on earthquake-induced landslide triggering. Landslides 12:335–344
Yuan R et al (2016) Newmark displacement model for landslides induced by the 2013 Ms 7.0 Lushan earthquake, China. Front Earth Sci 10: 740–750
Zeghouane H, Allek K, Kesraoui M (2016) GIS-based weights of evidence modeling applied to mineral prospectivity mapping of Sn-W and rare metals in Laouni area, central Hoggar, Algeria. Arab J Geosci 9:1–13
Zêzere JLs, de Brum Ferreira A, Rodrigues MLs (1999) The role of conditioning and triggering factors in the occurrence of landslides: a case study in the area north of Lisbon (Portugal). Geomorphology 30:133–146
Zhang D, Agterberg F, Cheng Q, Zuo R (2014) A comparison of modified fuzzy weights of evidence, fuzzy weights of evidence, and logistic regression for mapping mineral prospectivity. Math Geosci 46:869–885
Zhang G et al (2016a) Integration of the statistical index method and the analytic hierarchy process technique for the assessment of landslide susceptibility in Huizhou, China. CATENA 142:233–244
Zhang Z et al (2016b) GIS-based landslide susceptibility analysis using frequency ratio and evidential belief function models. Environ Earth Sci 75:1–12